

Research Report: Regular Manuscript

# Cerebral Dopamine Neurotrophic Factor regulates multiple neuronal subtypes and behavior

https://doi.org/10.1523/JNEUROSCI.2636-19.2020

Cite as: J. Neurosci 2020; 10.1523/JNEUROSCI.2636-19.2020

Received: 6 November 2019 Revised: 23 June 2020 Accepted: 25 June 2020

This Early Release article has been peer-reviewed and accepted, but has not been through the composition and copyediting processes. The final version may differ slightly in style or formatting and will contain links to any extended data.

Alerts: Sign up at www.jneurosci.org/alerts to receive customized email alerts when the fully formatted version of this article is published.

Copyright © 2020 the authors



3

5

Yu-Chia Chen <sup>1</sup> , Diego Baronio <sup>1</sup> , Svetlana S	Semenova <sup>+</sup> . Shamsijat Abdurakhmanova <sup>+</sup>	. Pertti Panula¹*
---	---	-------------------

- 4
  - <sup>1</sup>Department of Anatomy, University of Helsinki, Finland

# 6

- 7 \*Correspondence: Professor Pertti Panula
- 8 Department of Anatomy
- 9 University of Helsinki
- 10 POB 63
- 11 00014 University of Helsinki
- 12 Finland
- 13 Tel: +358-40-5922323
- 14 E-mail pertti.panula@helsinki.fi
- 15
- 16 Number of pages: 46 Number of figures: 13, Number of tables: 2
- 17 Number of words of abstract: 200; in introduction: 606; in discussion: 1491
- 18 Conflict of interest: The authors declare that no conflict of interest exists

# 19 Acknowledgements

- 20 This study was supported by grants from the Jane and Aatos Erkko Foundation, Sigrid Juselius Foundation,
- 21 Magnus Ehrnrooth's Foundation and Finska Läkaresällskapet. We thank Mr. Henri Koivula (BSc), Ms Riikka
- 22 Pesonen (BSc), and Ms. Noora Hellen (MSc) for expert technical help. We thank Dr. Mart Saarma, Dr. Esa
- 23 Korpi and Dr. Marnie Halpern for constructive comments on the manuscript. Zebrafish experiments were
- 24 carried out at the Zebrafish Unit of HiLife Infrastructures funded in part by Biocenter Finland.



# 25 Abstract

Cerebral Dopamine Neurotrophic Factor (CDNF) protects dopaminergic neurons against toxic damage in 26 27 the rodent brain and is in clinical trials to treat Parkinson's disease patients. Yet the underlying mechanism 28 is poorly understood. To examine its significance for neural circuits and behavior, we examined the 29 development of neurotransmitter systems from larval to male adult mutant zebrafish lacking cdnf. 30 Although a lack of *cdnf* did not affect overall brain dopamine levels, dopaminergic neuronal clusters 31 showed significant abnormalities. The number of histamine neurons that surround the dopaminergic 32 neurons was significantly reduced. Expression of tyrosine hydroxylase 2 in the brain was elevated in cdnf 33 mutants throughout their lifespan. There were abnormally few GABA neurons in the hypothalamus in the 34 mutant larvae, and expression of glutamate decarboxylase was reduced throughout the brain. cdnf mutant 35 adults showed a range of behavioral phenotypes, including increased sensitivity to pentylenetetrazoleinduced seizures. Shoaling behavior of mutant adults was abnormal, and they did not display social 36 37 attraction to conspecifics. CDNF plays a profound role in shaping the neurotransmitter circuit structure, 38 seizure susceptibility, and complex behaviors in zebrafish. These findings are informative for dissecting the 39 diverse functions of this poorly understood factor in human conditions related to Parkinson's disease and 40 complex behaviors.

41

# 42 Significance Statement

43

A zebrafish lacking cdnf grows normally and shows no overt morphologic phenotype throughout the life
 span. Remarkably, impaired social cohesion and increased seizure susceptibility was found in adult *cdnf* KO
 fish conceivably associated with significant changes of dopaminergic, GABAergic and histaminergic systems
 in selective brain areas. These findings suggest that cdnf has broad effects on regulating neurogenesis and



49 than ones restricted to the dopaminergic systems.

50

48

# 51 Introduction

52

Neurotrophic factors (NTFs), such as neurotrophins, glial cell line-derived neurotrophic factor family of ligands, and neurokines are crucial regulators of neurogenesis and regeneration. These secretory proteins and their signaling receptors are responsible for the survival, maintenance, and synaptic plasticity of nervous systems (Chao, 2003). Several neurodegenerative disorders such as Parkinson's disease (PD) and Alzheimer's disease (AD) are associated with dysregulation of trophic factors (Chao et al., 2006; Mitre et al., 2017).

59

60 An unconventional NTF family, which has a distinct two-domain protein structure and trophic effects on 61 dopaminergic neurons, has recently been identified (Parkash et al., 2009; Latge et al., 2015). This 62 evolutionarily conserved NTF family contains two proteins - mesencephalic astrocyte-derived neurotrophic factor (MANF) and cerebral dopamine neurotrophic factor (CDNF)(Lindahl et al., 2017). Their protein 63 structure contains two main functional motifs. One is the N-terminus, which is similar to the saposin-like 64 65 domain that has the capacity of lipid/cell membrane binding. The other is the C-terminus, composed of the 66 unfolded Cys-X-X-Cys (CXXC) motif, the SAP domain of Ku70, and a putative endoplasmic reticulum (ER) 67 retention signal (KDEL/RTDL) at the end of the C-terminal, which may protect cells from ER stress-induced 68 apoptosis (Parkash et al., 2009; Latge et al., 2013; Latge et al., 2015). Both CDNF and MANF are detectable 69 mainly in neurons in adult mouse and human brain, whereas the expression level of CDNF is generally 70 lower than that of MANF (Lindholm et al., 2007; Lindahl et al., 2017). CDNF and MANF both protect

3



induced neuronal death (Liu et al., 2015; Lindahl et al., 2017; Sousa-Victor et al., 2018). As such, CDNF has
become recognized as a promising candidate for clinical treatment of PD due to its potent neuroprotective
and neurorestorative effects on midbrain dopamine neurons (Lindholm et al., 2016; Lindahl et al., 2017;
Nasrolahi et al., 2018).

dopaminergic neurons against oxidative stress, neurotoxins, cerebral ischemia, and neuroinflammation-

76

71

77 CDNF protects cultured mesencephalic neurons against alpha-synuclein-oligomer-induced toxicity (Latge et 78 al., 2015). In 6-hydroxydopamine (6-OHDA) and 1-methyl-4-phenyl-1,2,3,6-tetrahydropyridine (MPTP)-79 induced Parkinsonian animal models, the application of CDNF and MANF protects and rescues midbrain 80 dopamine neurons (Lindholm et al., 2007; Voutilainen et al., 2011; Airavaara et al., 2012; Ren et al., 2013). 81 In addition to its neuroprotective effects in PD animal models, CDNF improves long-term memory in an 82 APP/PS1 mouse model of AD (Kemppainen et al., 2015), and reduces AB25-35-induced ER stress and 83 synaptotoxicity in cultured hippocampus neurons (Zhou et al., 2016). Growing evidence suggests that 84 MANF and CDNF are ER stress response proteins involved in the unfolded protein response (UPR) through 85 interactions with glucose-regulated protein 78 (BiP/GRP78) (Arancibia et al., 2018; Yan et al., 2019). 86 Nevertheless, how CDNF responds to ER stress and its functions under healthy conditions remain largely 87 unknown (Lindahl et al., 2017).

88

The role of CDNF in the development of dopaminergic or other neurons has not been addressed. The role and mechanisms of action of CDNF have remained elusive. To examine the biological function of cdnf and its role in neural systems and behavior, we first generated zebrafish null mutants by CRISPR/Cas9 genome editing. We investigated the role of cdnf on major neurotransmitter systems in the CNS, including dopaminergic, histaminergic, serotonergic, and GABAergic circuits using qPCR, *in situ* hybridization,



immunohistochemistry, and HPLC analysis, as well as locomotor behavioral analysis, from development throughout their life span. We found that adult *cdnf* mutant zebrafish show abnormal social behaviors and seizure susceptibility phenotypes that are conceivably associated with the multiple impairments of major neurotransmitter networks and deficient neural progenitors during embryonic neurogenesis. These results may provide new evidence that CDNF has a considerable impact on neurogenesis and formation of normal neurotransmitter systems in CNS, which may have important implications for human neurological

100 disorders.

94

95

96

97

98

99

5



# 101 Materials and Methods

## 102 Zebrafish Maintenance

103 Zebrafish were obtained from our wild-type (Turku) line that has been maintained in the laboratory for 104 more than a decade (Kaslin and Panula, 2001; Sundvik et al., 2011; Chen et al., 2016). Larvae were raised on 105 14:10 (light:dark, lights on at 8 a.m.) cycles at 28°C and fed daily once with flake food and two times with live artemia. Adult fish were raised in continuously cycling Aquatic Habitats<sup>™</sup> systems (Apopka, FL, USA) 106 107 with complete exchange of water in each tank every 6-10 min. Circulating water was UV sterilized, filtered 108 with foam filters and activated charcoal. Water quality, including temperature (28±0.5°C), pH value  $(7.4\pm0.2)$  and conductivity  $(450\pm10\mu S)$  was monitored continuously. Embryos were obtained by natural 109 110 spawning, collected from the breeding tanks and staged in hours post-fertilization (hpf), days post-111 fertilization (dpf), or months post-fertilization (mpf) as previously described (Kimmel et al., 1995). The permits for all experiments were obtained from the Office of the Regional Government of Southern 112 113 Finland, in agreement with the ethical guidelines of the European convention.

114

<u>JNeurosci Accepted Manuscript</u>

# 115 RNA isolation and cDNA synthesis

Total RNA was extracted from ten pooled larval fish or one dissected adult brain per sample (RNeasy mini Kit; Qiagen, Valencia, CA, USA) for quantitative RT-PCR (qRT-PCR). To synthesize cDNA, 2µg of total RNA was reverse-transcribed using SuperScriptTM III reverse transcriptase (Invitrogen, Carlsbad, CA, USA) with random hexamer primers (Roche Diagnostics, Germany) according to the manufacturer's instructions.

120

121 In Situ Hybridization

6

122	Whole-mount in situ hybridization (WISH) was performed on 4% paraformaldehyde (PFA)-fixed embryos
123	and dissected brains as described earlier (Chen et al., 2009). Antisense and sense digoxigenin (DIG)-labelled
124	RNA probes were generated using the DIG RNA labelling kit (Roche Diagnostics, Germany) following the
125	manufacturer's instructions. The WISH procedure was followed according to the protocol described by
126	Thisse & Thisse (Thisse and Thisse, 2008), with slight modifications. Briefly, the prehybridization and
127	hybridization steps were conducted at 60°C for all riboprobes. The specificity of the anti-sense riboprobe
128	hdc and th2 have been described earlier (Chen et al., 2009; Chen et al., 2016). The cloning primers for the
129	open-reading frames of <i>cdnf</i> and <i>vGAT</i> cDNA are listed in Table 1. <i>In situ</i> hybridization signals were
130	detected with sheep anti-digoxigenin-AP Fab fragments (1:10,000; Roche Diagnostics, Germany). The color
131	staining was carried out with chromogen substrates (nitro blue tetrazolium and 5-bromo-4-chloro-3-
132	indolyl-phosphate) and incubated in the dark at room temperature. Stained samples were embedded in
133	80% glycerol and visualized under brightfield optics using a Leica DM IRB inverted microscope with a DFC
134	480 charge-coupled device camera. Z-stacks were processed with Leica Application Suit software, with the
135	multifocal algorithm to identify the gene expression patterns (Chen et al., 2012).

# 137 Quantitative real-time PCR (qPCR)

138 qPCR was performed with a LightCycler<sup>®</sup> 480 instrument (Roche, Mannheim, Germany) using the 139 Lightcycler<sup>®</sup>480 SYBR Green I master mix (Roche, Mannheim, Germany) according to the manufacturer's 140 instructions. Primers for amplification were designed by Primer-BLAST (NCBI) and are listed in Table 1. Two 141 housekeeping genes,  $\beta$ -actin and ribosomal protein L13a (rpl13a) were used as reference controls. All 142 primer sets were confirmed to amplify only a single product of the correct size. Cycling parameters were as 143 follows: 95°C for 5 min, followed by 45 cycles of 95°C for 10 s, 60°C for 15 s, and 72°C for 20 s. Fluorescence changes were monitored with SYBR Green after every cycle. Dissociation curve analysis was 144 145 performed at the end of the cycles (0.1°C per s increase from 60°C to 95°C with continuous fluorescence



readings) to ensure that only a single amplicon (single melting peak) was obtained. All reactions were performed in duplicates, and at least three individual biological replicates were used (sample numbers indicated in figure legends). Duplicate quantification values were analyzed with the LightCycler 480 software. The data were calculated by the comparative method, using Ct values of  $\beta$ -*actin* and *rpl13a* as a reference control (Livak and Schmittgen, 2001). Since the changes of relative gene expression showed the same trend when normalized to the different housekeeping genes (data not shown), only the results from *rpl13a* are presented.

153

## 154 Establishing zebrafish mutants

155 CRISPR/Cas9-genome edited fish were generated in our Turku wild-type strain, based on the description of Hwang et al. (Hwang et al., 2013). To avoid off-target genomic mutagenesis effects, targeting sites were 156 157 selected with a minimum of three mismatches in the genome as predicted by the CHOPCHOP software 158 (http://chopchop.cbu.uib.no). The sequence-specific sgRNA template was generated in a pDR274 vector 159 (Addgene Plasmid #42250; oligo sequence listed in Table 1). The sequences of the modified plasmids were 160 verified by Sanger sequencing. sgRNAs were transcribed from linearized template plasmids (Ambion 161 MEGAscritp), and Cas9 mRNA was transcribed in vitro from linearized template plasmid pMLM 3613 (Addgene Plasmid #42251). A mixture containing approximately 300ng/µl Cas9 mRNA and 20ng/µl sgRNA 162 163 was injected into fertilized eggs at the one-cell stage. To verify the mutation efficiency of Cas9-sgRNA 164 genome editing, the injected eggs were collected at 24 hpf. DNA was extracted from individual embryos 165 and non-injected controls. PCR amplicons encompassing the targeted sites were amplified and analyzed via 166 Sanger sequencing and high-resolution melting (HRM) analysis (Roche, Mannheim, Germany). Mutations 167 were recognized as multiple sequencing peaks at the sgRNA target site. When the mutation efficiency was 168 over 50%, the remaining Cas9/sgRNA-injected embryos were raised to adulthood and out-crossed to the 169 wild-type fish to generate F1 progeny. To collect the tail biopsies, 3-dpf embryos were anesthetized with

8



170 0.02% Tricaine. The tip of the caudal fin within the pigment gap was removed using a microscalpel, and 171 each larva was placed in an individual well of a 24-well plate with fresh embryonic medium until 5 dpf. We 172 have consistently achieved 100% survival rate from the beginning of this procedure to adulthood. F1 genotyping was done by HRM assays and DNA sequencing. To identify mutated alleles from single embryos, 173 174 each target locus was PCR amplified from individual genomic DNA with gene-specific primers (Table 1). PCR 175 products were then cloned and sequenced. Mutated alleles were identified by comparison with the wild-176 type sequence. Heterozygous (HET) F1 siblings carrying the same mutations were pooled in one tank and 177 raised to adulthood. Due to the sex imbalance in the F1 generation of cdnf HET fish, F1 male HET fish were 178 outcrossed to Turku female wild-type fish; female mutants were obtained from the resulting F2 progeny. Genotyping of the F2s was done as described for the F1 generation. 179

180

## 181 Fin clipping and genomic DNA extraction of adult zebrafish and 3 dpf larvae

182 To lyse genomic DNA, individual tail clippings were incubated in 50µl lysis buffer (10mM Tris-HCl pH8.3, 183 50mM KCl, 0.3% Tween-20 and 0.3% NP-40) at 98°C for 10 min, followed by incubation on ice for 2 min. 1µl 184 of Proteinase K (20mg/ml) was added to remove protein, and the mixture was incubated at 55°C for at least 4 h. To inactivate Proteinase K activity, samples were incubated at 98°C for 10 min and quenched on 185 186 ice. To detect indel mutations, HRM curve acquisition and analysis was performed. Primers flanking the 187 mutation site were designed using Primer-BLAST (https://www.ncbi.nlm.nih.gov/tools/primer-blast; 188 sequences are listed in Table 1). The HRM analysis was performed on a LightCycler® 480 instrument 189 (Roche) using the following reaction mixtures: 1× LightCycler 480 HRM master mix (Roche, Mannheim, 190 Germany), 2mM MgCl<sub>2</sub>, and 0.15µM primer mixtures. The PCR cycling protocol was as follows: one cycle of 95°C for 10 min; 45 cycles of 95°C for 10 s, 60°C for 15 s, 72°C for 20 s, and melting curve acquisition; one 191 192 cycle of 95°C for 60 s, and 40°C for 60 s. PCR products were denatured at 95°C for 60 s, renatured at 40°C 193 for 60 s, and melted at 60°C to 95°C with 25 signal acquisitions per degree. Melting curves were generated 9



194 over a 65–95°C range. Curves were analyzed using the LightCycler® 480 gene-scanning software (version 195 1.5) according to the manufacturer's instructions (Roche Diagnostics Ltd., Switzerland). To identify 196 deviations of the curves indicative of sequence mutations, a three-step analysis was performed using the 197 Gene Scanning program (Roche) as follows: (1) Normalizing the raw melting-curve data by setting the initial 198 fluorescence uniformly to a relative value of 100% and the final fluorescence to a relative value of 0%. (2) 199 Determining the temperature threshold at which the entire double-stranded DNA was completely 200 denatured. (3) Further analyzing the differences in melting-curve shapes (threshold setup 0) in order to 201 cluster the melting curves with similar shapes into the same groups. Those with analogous melting curves 202 were characterized as the same genotype.

203

# 204 Analysis of catecholamines and histamine by high performance liquid chromatography (HPLC)

For each sample, ten 8-dpf larvae were pooled into a group. The dissected brains of 8-mpf or 18- males
were flash-frozen in liquid nitrogen and individually homogenized with sonication in 150µl of 2% perchloric
acid. After centrifugation, 10µl of supernatant was assessed for monoamine concentration measurement.
The detection details are described in Sallinen et al. (Sallinen et al., 2009). The results were normalized to
the total protein concentration of each sample, which was measured using the Pierce<sup>®</sup> BCA Protein Assay
Kit. The HPLC analysis was carried out as a blinded experiment.

211

## 212 Immunocytochemistry

Immunostaining was performed on zebrafish fixed in 2% PFA or 4% 1-ethyl-3 (3-dimethylaminopropyl) carbodiimide (EDAC, Carbosynth, Berkshire, UK). For larvae older than 5 dpf, fixed brains were dissected to
 enhance antigen presentation and improve image quality. Antibody incubations were carried out with 4%
 normal goat serum and 1% dimethyl sulfoxide (DMSO) in 0.3% Triton X-100/ phosphate buffered saline



217 (PBS) for 16 h at 4°C with gentle agitation. Primary antibodies were mouse monoclonal anti-tubulin,

acetylated antibody (1:1000; T6793, Sigma, St. Louis, MO, USA), rabbit anti-histamine 19C (1:5,000; (Panula

et al., 1990; Sundvik et al., 2011), rabbit anti-TH2 antibody (1:2000; (Semenova et al., 2014), rabbit anti-

220 serotonin antibody (1:1000; S5545, Sigma, St. Louis, MO, USA), anti-tyrosine hydroxylase (TH1) monoclonal

221 mouse antibody (1:1000; Product No 22941, Immunostar, Husdon, WI, USA), anti-GABA 1H (1:1000;

(Karhunen et al., 1993; Kukko-Lukjanov and Panula, 2003), rabbit anti-orexin A (1:1000;

223 Millipore/Chemicon, Billerica, MA, USA) and mouse anti-zrf1 (Gfap; 1:1000, Zebrafish International

224 Resource Center). The specificities of the anti-GABA (Karhunen et al. 1993) and anti-histamine, commercial

225 anti- mouse monoclonal TH, anti-rabbit-TH2 and anti-serotonin antibodies have been verified previously

(Kaslin and Panula, 2001). The following secondary antibodies were applied: Alexa Fluor® 488 and 568 anti-

227 mouse or anti-rabbit IgG (1:1000; Invitrogen, Eugene, OR, USA).

228

## 229 Immunocytochemistry following EdU proliferation labeling

To detect the proliferating S-phase dividing cells, the Click-iT<sup>™</sup>EdU Alexa Fluor 488 imaging kit (Molecular 230 231 Probes) was used following the manufacturer's instructions, with minor modifications. Briefly, 5-dpf larvae were incubated in 0.5mM EdU/E3 buffer (zebrafish embryonic medium; 5 mM NaCl, 0.44 mM CaCl<sub>2</sub>, 0.33 232 mM MgSO<sub>4</sub>, and 0.17 mM KCl) with 1% DMSO for 24 h at 28°C. Labelled samples were transferred back to 233 E3 medium for 30 min and fixed in 4% EDAC/PB buffer pH 7.0 overnight at 4°C with gentle agitation. The 234 skin and lower jaw of the fixed specimens were removed in order to enhance sample penetration. 235 236 Dissected brains were incubated with rabbit anti-Histamine 19C antibody (1:5000) and mouse anti-HuC antibody (1:1000). The secondary antibody Alexa Fluor®568 anti-rabbit IgG and Alexa Fluor®633 anti-mouse 237 238 IgG (1:1000; Invitrogen, Eugene, OR, USA) were applied. After immunostaining, labelled specimens were 239 fixed in 4% PFA/PB for 20 min at room temperature, and then incubated in 1× Click-iT EdU cocktail with the 240 green-fluorescent Alexa Fluor® 488 azide dye for one hour in the dark at room temperature. After removing 11



for 10 min, samples were mounted in 80% glycerol/PBS for confocal microscopy imaging.

243

241

## 244 Imaging

245 Brightfield images were taken with a Leica DM IRB inverted microscope with a DFC 480 charge-coupled 246 device camera. Z-stacks were processed with Leica Application Suite software and Corel DRAW 2018 software (Chen et al., 2009). Immunofluorescence samples were examined using a Leica TCS SP2 AOBS 247 248 confocal microscope. For excitation, an Argon laser (488 nm), green diode laser (561 nm), and red HeNe 249 laser (633 nm) were used. Emission was detected at 500–550 nm, 560–620 nm, and 630–680 nm, respectively. Cross-talk between the channels and background noise were eliminated with sequential 250 251 scanning and frame averaging as previously described (Sallinen et al., 2009). Stacks of images taken at 0.2-252 1.0 µm intervals were compiled, and the maximum intensity projection algorithm was used to produce final 253 images with Leica Confocal software and Imaris imaging software (version 6.0; Bitplane AG, Zurich, 254 Switzerland). Cell numbers were counted in each 1.0 µm optical slice using ImageJ 1.52b software (National 255 Institutes of Health, Bethesda, USA). Fluorescence intensity was quantified in each 1.0 µm optical slice 256 across entire z-slices with a standardized-selected region of interest (ROI) under the same parameters using 257 ImageJ 1.52b software. All cell counts and fluorescence intensity measurements were performed by an 258 investigator blinded to the sample type.

259

# 260 Estimation of the posterior swimbladder volume (V3)

The volume of the posterior chamber V3 region (geometrical figure like frustum of a con) was estimated according to the equation (V =  $(1/3) *\pi * h * (r1^2 + r2^2 + (r1 * r2))$  as described in detail in Lindsey et al. (Lindsey et al., 2010). Measurements were done on 6-month-old male zebrafish (n=4 of both genotypes)



using Fiji (version 2.0) and were calculated using the lateral-aspect images of the 4% PFA-fixed posterior
 chamber.

266

## 267 Estimation of the vascular length density of the posterior swimbladder

The vascular length density was estimated using the vessel analysis plugin with Fiji (version 2.0) based on the user manual. The calculation of the vascular length density was presented as the ratio of skeletonized vasculature area to the total area (% Area)(Elfarnawany, 2015). Measurements were done on the lateralaspect images of the 4% PFA-fixed posterior chamber of 6-month-old male zebrafish (n=4 of both genotypes).

273

## 274 Dark-light flash and sleep behavior test for larval zebrafish

275 Behavioral trials were done between 11:00 and 16:00. For larval locomotion tracking, 6-dpf zebrafish larvae 276 were individually placed in a 24-well culture dish well containing approximately 1.5mL of E3 medium. The 277 light level was set to approximately 330 lux based on the setting of Puttonen et al. (Puttonen et al., 2018). 278 Before each trial, the larvae were habituated in the observation chamber for 10 min, followed by a 30 min 279 locomotion tracking period with the lights on. A dark-light flash response was induced by switching off the 280 lights for 2 min, then turning them back on for 2 min. One experiment consisted of three subsequent 281 periods of white lights on and white lights off. Locomotor activity was monitored for one day with 282 continuous illumination by infrared lights while white light remained on from 12:00 to 22:00 on the first 283 day and from 8:00 to 12:00 on the next day. Locomotion response was monitored at room temperature 284 using the Daniovision system (Noldus, Wageningen, The Netherlands). Video tracking was analyzed by 285 EthoVision XT 8.5 locomotion tracking software (Noldus, Wageningen, The Netherlands).



## 287 Social interaction assay

288 The visually mediated social preference test was based on the setup of Baronio et al. (Baronio et al., 2018). 289 Briefly, an acrylic apparatus (29 cm length × 19 cm height × 29 cm width) was divided into three arenas by 290 two acrylic partitions. A rectangular compartment in the middle was the testing arena, referred to as the 291 "distal" zone; to one side, the conspecific compartment housed a group of six fish, referred to as the 292 "stimulus" zone; the other adjacent compartment was filled with stones and plant mockups, referred to as 293 the "object" zone. A single 6-mpf male adult was placed in the testing arena to allow exploration and 294 analysis of place preference. All experimental fish were raised in a social environment. All behavioral tests 295 were performed between 11:00 and 16:00, and video-recorded from above the tank for 6 min. To quantify 296 social preference, the videos were analyzed with the EthoVision XT 8.5 locomotion tracking software 297 (Noldus, Wageningen, The Netherlands), and the amount of time each test fish spent in the proximity of 298 each compartment was quantified.

299

## 300 Novel diving tank assay

301 The novel tank assay was performed based on Cachat et al. (Cachat et al., 2010). One day before the 302 experiment, 6-mpf male adult fish with home tanks (19 cm x 34 cm x 21 cm) were habituated in the 303 behavior testing room. In each trial, one fish was placed in a transparent tank (24 cm × 14.5 cm × 5 cm) 304 with 1 L of fish system water. All behavioral tests were performed between 11:00 and 16:00, and video-305 recorded from the side of the tank for 6 min, using a Basler acA1300-60gm industrial CCD video camera. 306 We performed a three-compartment novel tank test, with digitized divisions between top, bottom, and 307 middle virtual zones. The time spent in each zone was quantified using EthoVision XT 8.5 software. Fish 308 were returned to their home tanks immediately after the test.



# 310 Shoaling assay

309

311 Five 6-mpf or five 18-mpf male fish per cohort were placed in a round white polyethlene plastic flat-312 bottomed container (23 cm height, 23 cm diameter) with 2 L of fish system water (5.0 cm depth) based on 313 the description of Green et al. (Green et al., 2012). Prior to testing, fish were habituated for 15 min followed 314 by video recording for 10 min with a camera at a fixed height (60 cm) from the top of the container. All 315 videos were analyzed with EthoVision XT 8.5 software, using the default setting (the center-point detection 316 of the unmarked animals). The mean of the inter-fish distance (defined as distance between the body 317 center of every member of the shoal) (Green et al., 2012) was quantified from the average data from all 318 trials (n=4 trials for the 6-mpf fish, and n=3 trials for the 18-mpf fish). The proximity duration (in s) was 319 defined as the average duration of time a fish stayed close to the shoal fish (i.e. within 2 cm for the 6-mpf 320 fish or 2.5 cm for the 18-mpf fish). The misdetection rate of the video-tracking software was less than 1%. 321 All behavioral trials were done between 11:00 and 16:00.

322

## 323 Seizures induced by pentylenetetrazole (PTZ) in adult zebrafish

Epileptic seizure stage scores (seizure behavior scores from 0 to 6) were assigned according to Mussulini et 324 325 al.(Mussulini et al., 2013). 6-mpf male fish were individually exposed to 10 mM PTZ in a 1 L tank (24 cm 326 length × 5 cm width × 14.5 cm height) for 5 min on three consecutive days, in order to induce experimental 327 seizures based on the description of Duy et al. (Duy et al., 2017). After PTZ administration and seizure 328 analysis, treated fish were transferred to a clean tank for one day until they recovered (i.e. seizure score = 329 0). They were then sacrificed by decapitation after cold-shock, and brains were dissected for RNA 330 extraction. The PTZ concentration and the exposure period were selected and optimized based on our pilot 331 study, which aimed to determine the shortest time of PTZ exposure that induces a seizure of score V



332 (including fish falling to the bottom of the tank and loss of the body posture for 1-2 s), but allowing full 333 recovery after three daily exposures (Duy et al., 2017). Control fish were subjected to the same procedure 334 but exposed to only clean system water.

335

#### 336 **Experimental design and Statistical analysis**

337 The number of zebrafish for all experiments is indicated in the figure legends. Data analysis was performed

- 338 by GraphPad Prism software (version 7; San Diego, CA, USA). Two-tailed p-values were generated by one-
- 339 way analysis of variance (ANOVA) for multiple comparisons using Tukey's multiple comparison test, two-
- 340 way ANOVA for multiple comparisons, and Student's unpaired t-test for comparison of two groups. Data
- 341 were presented as mean ± SEM. Statistical significance was considered at p-value <0.05.



🖅 Made Will Pdf Office

# 342 Results

### 343 Zebrafish cdnf 3D structure and mRNA distribution during embryogenesis and in adult tissues

Currently there is one human homologous cdnf (NM 001123281.1) documented in the latest zebrafish 344 345 database (GRCz11). The zebrafish cdnf gene is located on chromosome 4 and contains four exons with the 346 exon-intron splice sites conserved in mammalian CDNF and MANF. The open reading frame encodes a 347 protein of 182 amino acid residues with a 25 amino-acid signal peptide and shares 67.4% and 65.1% of 348 amino acid sequence similarity with zebrafish manf (NP\_001070097) and human CDNF (NP\_001025125), 349 respectively. The predicted secondary structure analyzed by the protein homology/analogy recognition 350 engine Phyre2 (Kelley et al., 2015) indicated that zebrafish cdnf contained seven  $\alpha$ -helices (Figure 1A) and 351 eight positioned-conserved cysteine residues. The N-terminus domain is highly similar to human saposin D, 352 and the C-terminus is analogous to the SAP domain (Figure 1B), suggesting that zebrafish cdnf is structurally 353 conserved with human CDNF (Latge et al., 2013). To determine the spatiotemporal expression of cdnf, WISH and qPCR was performed in embryos and adult tissues. The *cdnf* mRNA was widely expressed at 1 dpf 354 355 in the brain, eyes, and muscles. In 2- and 3-dpf larvae, cdnf transcripts were detected in the midbrain-356 hindbrain boundary, hindbrain, otic vesicles, and heart (Figure 1C). qPCR detected cdnf transcripts as early 357 as 2 hpf (Figure 1D), and expression gradually increased after 1 dpf. In adult organs, the highest expression 358 level was found in the eyes compared with the brain, kidney, and liver; no sex differences were detected 359 (Figure 1E).

360

# 361 Characterization of the CRISPR/Cas9-generated zebrafish cdnf mutant allele

To study the biological function of *cdnf*, we generated mutations using the CRISPR/Cas9 system. A sequence-specific guide RNA was designed to target exon2 of *cdnf* (Figure 2A). We identified two reading frame-shift mutant alleles: one with a 14 base-pair deletion (Figure 2A and 2B) and another with a 1 base-



365 pair insertion (data not shown). Both lesions are located in exon2, causing premature termination of the 366 protein after amino acid 49 (NP 001116753.1, Figure 2B). We also cloned and sequenced the full-length 367 reading frame in *cdnf* transcripts isolated from the mutant brain. The deletion sequence was the same as the genomic deletion sequence. In this study, the cdnf 14 base-pair deletion mutant allele was used for 368 369 subsequent experiments. Heterozygous cdnf mutants (F3 and later generations) were mated to generate 370 wild-type (WT), heterozygous (HET), and homozygous mutant embryos. The ratio of genotyped sibling 371 offspring matched the normal Mendelian ratio (1:2:1). All progenies were tail clipped at 3 dpf and 372 genotyped using HRM analysis, according to the distinct melting curves of each genotype. The embryos 373 with the same HRM curve were grouped together before 5 dpf (Figure 2C). In situ hybridization results 374 revealed that *cdnf* expression was mostly abolished in the caudal raphe, ventral part of the posterior 375 tuberculum, tectum opticum and ventricular recess of the hypothalamus of cdnf mutant brains (Figure 2D, 376 2E). The faint signal in the cdnf mutant brain may be due to the remaining truncated mRNA. The cdnf 377 mRNA quantification is shown in Figure 3A-3C. cdnf homozygous mutants were viable, swam normally, 378 were fertile, and had no gross morphological phenotype (Figure 2F).

379

# 380 Upregulation of tyrosine hydroxylase 2 (th2) expression in cdnf mutant fish

381 We addressed the question whether *cdnf* is required for development or maintenance of the dopaminergic neurons in the zebrafish brain. qPCR analysis was performed on 8-dpf larvae, 8-mpf brains, and 18-mpf 382 383 brains to examine transcript levels of relevant marker genes of the dopaminergic and histaminergic systems 384 (known to depend on dopaminergic system). manf was also analyzed to reveal if this closely related growth 385 factor is upregulated as a consequence of genetic compensation in the *cdnf* mutant fish. In zebrafish, gene 386 duplication has led to two non-allelic forms of human orthologous tyrosine hydroxylase (th) that are 387 expressed in the brain in a largely complementary manner (Chen et al., 2009). We thus analyzed the mRNA 388 levels of both tyrosine hydroxylases, th1 and th2. Remarkably, a significant increase of th2 was observed in 18



*cdnf* mutants compared with their WT siblings (Figure 3D-3F), whereas the expression level of *th1* mRNA showed no statistically significant difference (Figure 3G-3I). Additionally, a significant downregulation of *histidine decarboxylase* (*hdc*, a histaminergic marker) transcript was observed in 8-mpf mutant brains

(Figure 3J-3L). Expression of *hdc* has been shown to be regulated by dopamine produced by *th2* (Chen et
al., 2016). We also confirmed that a significant reduction of *cdnf* transcript remained in *cdnf* mutants
throughout their lifespan (Figure 3A-3C), which agreed with the *in situ* hybridization results (Figure 2D, 2E)
that most of the truncated *cdnf* mRNA went through nonsense-mediated mRNA decay pathway in *cdnf*deficient mutant fish. The mRNA level of *manf*, a closely related trophic factor, was not significantly altered
(data not shown). The qPCR results revealed that *cdnf* has an impact on the regulation of dopaminergic and
histaminergic gene expression.

399

389

390

391

## 400 A dynamic change of dopaminergic neuron numbers in *cdnf* mutant fish

401 It is evident that dopaminergic signaling regulates the developing hypothalamic neurotransmitter identity 402 (Chen et al., 2016). Due to the prominent upregulation of *th2* transcripts in *cdnf* mutant fish, we then 403 quantified the number of cells of the dopaminergic populations in the prethalamus and caudal 404 hypothalamus by immunohistochemistry to assess whether the TH1- and TH2-containing cell numbers 405 were altered. 8-dpf dissected brains were co-stained with two antibodies that recognize dopaminergic neurons; one recognizes both TH1 and TH2 (Semenova et al., 2014), and one recognizes only TH1 in 406 407 zebrafish. A significant increase in TH1- and TH2-positive cell numbers was observed in TH1/TH2 group 408 10/10b in the caudal hypothalamus area (Hc) of knock-out (KO) mutants compared with their WT siblings 409 (Figure 4A-4E). However, the number of TH1-positive cells was unaffected in this region (Figure 4F), 410 suggesting that the increase in TH1- and TH2-positive cell numbers in the Hc area of cdnf mutant brains is 411 due to the increase in TH2-containing neurons, consistent with the qPCR results (Figure 3D-3F) and the in 412 situ hybridization result (Figure 4J). Nevertheless, a significant decrease in TH1-positive cell number was



found in the prethalamus region (TH1 group 5,6,11) in *cdnf* mutants (Figure 4G). On the other hand, the
serotonergic population in this location remained intact in KO mutants (Figure 4H and 4I). A dynamic
change in dopaminergic neuron populations found in *cdnf* mutant fish suggests that *cdnf* may function
distinctly on dopaminergic populations in different brain areas.

417

## 418 Decreased number of proliferating cells and histaminergic neurons in *cdnf* mutant fish

419 There are no reports about *cdnf* effects on embryonic neurogenesis. We previously reported that the 420 dopaminergic populations in the caudal hypothalamus play a role in the regulation of histaminergic neuron 421 development in zebrafish (Chen et al., 2016). To investigate whether the loss of functional cdnf affects 422 neurogenesis and if the upregulated TH2 population in this area disturbs the development of histaminergic 423 neurons in larval cdnf mutants, we studied 8-dpf dissected brains co-stained with antibodies recognizing 1) 424 histamine (a histamine neuron marker), and 2) HuC (a panneuronal marker) following EdU staining (a 425 proliferation marker) (Figure 5A and 5B). A significant reduction of EdU-positive cells (Figure 5C) as well as 426 lower fluorescence intensity of HuC immunoreactivity (Figure 5D) was found in the caudal hypothalamus of 427 cdnf mutant fish brains. Moreover, sox2a (neural progenitor marker) mRNA expression level was 428 significantly downregulated in the cdnf mutant larvae (Figure 5H). Taken together, these findings suggest 429 that lack of *cdnf* significantly affects embryonic neurogenesis in the caudal hypothalamus. Similarly, a 430 significant decrease of histaminergic neurons was found in cdnf mutants (Figure 5E). Consistently, in situ hybridization of hdc (an enzyme converting L-histidine to histamine) showed a significant decrease in hdc-431 432 positive cell numbers in *cdnf* KO fish (Figure 5F). A significant decrease in the number of orexin-positive 433 cells also found in *cdnf* KO fish (Figure 5G). This result was in agreement with reports that the 434 histaminergic system regulates orexin neuron development in zebrafish (Sundvik et al., 2011).

435



## 436 Neurotransmitter profile by HPLC analysis

437 Due to the alterations of dopaminergic and histaminergic neurons in *cdnf* mutant fish, HPLC analysis was 438 performed to measure the concentration of dopamine, norepinephrine, serotonin, histamine, and their metabolites throughout the zebrafish lifespan. No statistically significant difference was found in brain 439 440 dopamine, norepinephrine, and serotonin levels, but a decrease in dopamine metabolites, DOPAC, and 441 homovanillic acid and serotonin metabolite 5-hydroxyindoleaetic acid was found in adult cdnf mutant fish 442 compared with the WT fish brains. (Table 2). A reduction in histamine level was found in 8-mpf cdnf 443 mutants, consistent with a reduced expression of histaminergic marker hdc mRNA in 8-mpf cdnf KO brains 444 (Figure 3K).

445

## 446 Impairments of GABAergic system

447 GABA acting through the GABA-A receptor in the adult brain is the major inhibitory neurotransmitter, and 448 GABAergic neurons are widely distributed in the brain to modulate neural activity. It has been reported 449 that MANF can potentiate presynaptic GABAergic inhibition (Zhou et al., 2006). Moreover, a dual 450 dopaminergic and GABAergic phenotype is evident in the hypothalamic areas in zebrafish (Filippi et al., 451 2014). Dopamine signaling deficiency affects the development of GABAergic neurons in zebrafish (Souza et 452 al., 2011). To assess whether the profound change of dopaminergic systems in *cdnf* mutant fish is 453 associated with abnormalities in the GABAergic system, anti-GABA and anti-acetylated-alpha-tubulin 454 antibodies (axonal alpha- tubulin marker) were used on 8-dpf dissected brains. Significantly fewer GABA-455 positive cells were observed in the ventral part of the posterior tuberculum (PTv) (Figure 6A-6C) and caudal 456 hypothalamus area (Hc) (Figure 6D) of the mutant fish than in their WT siblings. The axonal tubulin pattern 457 remained intact (Figure 6A, 6B and 6E) in cdnf mutants, suggesting that the loss of functional cdnf causes

21



specific abnormal neurotransmitter systems in the PTv and Hc areas rather than an overall change in
 neuronal organization.

460 GABA is converted from glutamic acid by glutamic acid decarboxylases (GADs: GAD65/gad2a and GAD67/gad1b), and vesicular GABA transporter (vGAT) is responsible for uptake and storage of GABA in the 461 462 vesicles in the presynaptic terminals. To study whether the decreased number of GABA-containing cells in 463 cdnf mutants stems from either dysfunction of GABA synthesis or neurotransmission, we performed gPCR 464 to determine the expression level of GABAergic markers slc32a1/vGAT, gad2a/gad65 and gad1b/gda67 in 465 8-dpf larvae. A significant decrease in *slc32a1/vGAT* transcripts was detected in *cdnf* mutant larvae (Figure 7A), and the in situ hybridization results of vGAT in 8-dpf dissected brains showed lower expression in the 466 467 ventral thalamus (VT), ventral part of posterior tuberculum (PTv) and hypothalamus (H) areas of cdnf KO 468 mutants than in their WT siblings (Figure 7B). However, the expression levels of gad1b, gad2a and vGlut2 in 469 whole larvae were not statistically different (Figure 7C-7E). These findings suggest that the decreased number of GABA-positive cells is associated with downregulation of vGAT expression in the cdnf KO larvae. 470

471

## 472 Dark-flash and sleep-related behavior

Dopaminergic, histaminergic, and GABAergic circuitries play important roles in the regulation of startle
response and sleep-wakefulness behavior (Jones, 2019). *cdnf* mutant larvae did not show impaired
light/dark adaptions by the light-dark flash change (data not shown). Therefore, we examined the sleep-like
locomotor behavior of 6-dpf larval fish under a 14:10 (light:dark) regime (Figure 8A, n=16 in each group).
Interestingly, during the daylight period, the *cdnf* mutant larvae were more active than their WT siblings
(Figure 8B) although locomotion during the second daylight period showed no statistically significant
differences between groups (Figure 8C). In contrast, during the dark period, the *cdnf* mutant larvae moved



481 and dark conditions was thus associated with the dysfunctional neurotransmission in *cdnf* mutant larvae.

482

480

## 483 Impaired social preference in adult cdnf mutant fish

484 There is growing evidence to suggest that dysregulated neurotransmission causes neuropsychiatric 485 disorders, some of which alter social interactions (Laruelle, 2014; Kim and Yoon, 2017; Provensi et al., 486 2018). Zebrafish are social animals and naturally tend to approach conspecifics by visual choice (Miller and 487 Gerlai, 2011). The social preference test conducted here measures this innate tendency. To investigate the 488 consequences of impaired dopaminergic, histaminergic, and GABAergic systems on adult fish behavior, we 489 performed social preference analysis/visually-mediated social preference on 6-mpf male fish by quantifying 490 the amount of time each fish spent in close proximity to conspecifics ("stimulus" arena) compared to the 491 empty "object" arena (Figure 9A). In comparison with their WT siblings, cdnf mutant fish spent significantly 492 less time in the stimulus/conspecific zone (Figure 9B and 9C), but spent more time in the "distal" testing zone (Figure 9B, 9E). WT and KO fish spent similar amounts of time in the "object" zone (Figure 9B, 9D), 493 494 indicating that adult *cdnf* mutant fish show less social preference for conspecifics than the WT fish.

495

# 496 Anxiolytic behavior appeared in adult *cdnf* mutant fish

Zebrafish have a natural tendency to spend more time at the bottom of the tank when placed in a novel environment, before gradually migrating to the surface (Kysil et al., 2017). We utilized a novel tank diving assay to study anxiety-related risk-taking behavior. The novel tank diving area was digitally divided into three zones, and representative swimming tracks are shown in Figure 10A. Compared with their WT siblings, *cdnf* mutants spent significantly more time exploring the top zone (Figure 10B, 10C), and less time in the bottom (Figure 10E); there was no difference in the time spent in the middle zone between WT and 23



KO siblings (Figure 10D). There was no significant difference for movement speed between WT and KO
siblings, suggesting that impaired bottom-dwelling behavior was not caused by motor defects (Figure 10F).
Moreover, buoyancy is regulated by the swim bladder and its innervation (Finney et al., 2006). We
examined the size of the swim bladder (Figure 10G, 10H), vasculature (Figure 10G, 10I) and TH1 innervation
(Figure 10G, 10J) of its posterior chamber, and no overt defect was found in the swim bladder of *cdnf* KO

508

509

## 510 Decreased shoal cohesion in adult cdnf mutant fish

fish (n=4 in each group).

511 Zebrafish swim naturally in shoals (Miller and Gerlai, 2011). To test whether cdnf deficiency affects fish 512 shoaling behavior, five 6-mpf fish (male young adult group) or five 18-mpf fish (male adult group) per trial were placed in a plastic cylindrical container (23 cm diameter, and monitored by video tracking for 10 min 513 514 after a 15 min habituation period (n=4 trials for young adults, and n=3 trials for adults). The movement 515 speed, average distance between the test fish and the other four shoal members, and duration of stays in 516 proximity (the nearest inter-individual distance defined as less than 2 cm for young adults and 2.5 cm for 517 adults) were analyzed. cdnf mutant fish showed higher swimming speed during 10 min locomotion activity 518 in both age groups (Figure 11A, 11B 11E, 11F). In the young adult group, the inter-individual distance was 519 significantly greater in the *cdnf* mutant group compared with their WT sibling group (Figure 11C). 520 Furthermore, the time spent in proximity with shoal members was significantly shorter in *cdnf* mutant groups than in their WT siblings (Figure 11D). Similar results were obtained in the adult group. Collectively, 521 522 the *cdnf* mutant fish were more hyperactive and kept at a greater distance to their neighbors (Figure 11G), 523 although no significant difference in time spent in proximity was observed in the adult group (Figure 11H), 524 suggesting that lack of functional *cdnf* causes social defect phenotypes in adult zebrafish.

525

24



527 We hypothesized that the impaired GABAergic phenotype found in the *cdnf* mutant fish may render the 528 mutants more susceptible to drug-induced epileptic seizures. Pentylenetetazole (PTZ), a chemoconvulsant drug, is commonly used to induce seizures in rodents and zebrafish by inhibiting GABA-A receptor subunits 529 530 (Huang et al., 2001; Mussulini et al., 2013). Six-month-old male fish were exposed to 10 mM PTZ (for 5 min 531 periods, over three consecutive days) to allow analysis of the molecular consequences of PTZ-induced 532 seizures (Figure 12A). Seizures were scored based on the description of Mussulini et al. (Mussulini et al., 533 2013). Briefly, score 3 was recorded when fish showed repetitive circular movements, score 4 included 534 abnormal whole-body rhythmic muscular contractions, and score 5 was characterized by rigidity, loss of 535 body posture, and sinking to the bottom of the tank. None of the tested fish died during the PTZ 536 administration procedure. Throughout the 5 min PTZ administration, a significantly higher percentage of 537 cdnf mutant fish reached score 5 compared to their WT siblings (Fig. 12B), revealing that cdnf mutant fish 538 are more susceptible to PTZ-induced seizures. Moreover, the cdnf mutant fish showed a shorter onset 539 latency to reach score 4 than their WT siblings, particularly on the second and third days of exposure 540 (Figure 12C). The *cdnf* mutant fish demonstrated the longest periods of immobility (Figure 12D), but there 541 were no significant differences between the genotypes in the total distance moved (Figure 12E).

542

# 543 Gene expression in PTZ-treated *cdnf* mutant and WT fish brains

To investigate the molecular alterations in the zebrafish brain caused by PTZ treatment, qPCR was used to quantify the gene expression of *manf* (a closely related growth factor), *glial fibrillary acidic protein* (*gfap*; an astrocyte marker), and GABAergic and glutamatergic markers. We first confirmed that 32% (Figure 13A) of the remaining *cdnf* truncated transcript was detected in untreated *cdnf* mutant fish brains compared with untreated adult *cdnf* WT fish brains, which agrees with the qPCR results on larvae (34%, Figure 3A). The



549 manf expression level did not alter significantly in untreated cdnf KO fish brains (Figure 13B). A significant 550 downregulation of slc17a6a/vGlut2, slc32a1/vGAT and gad2a/gad65 mRNA expression was observed in 551 untreated adult cdnf KO fish brains (Figure 13C, 13D and 13E), but not the expression level of gad1b/gad67 552 (Figure 13F). PTZ administration did not significantly alter the mRNA expression of cdnf, manf, GABAergic and glutamatergic markers in either WT or *cdnf* mutant fish (Figure 13A-13F), although there was a 553 554 tendency towards a higher level of mRNA expression of manf and GABAergic markers in PTZ treated cdnf 555 KO brains than in untreated cdnf KO fish group (Figure 13B-13F). Remarkably, mRNA expression of gfap 556 was significantly lower in untreated cdnf mutant fish brains than in WT fish brains (Figure 13G). After PTZ 557 treatment, a significant increase in gfap expression was seen in cdnf mutant fish brains, but not in their WT 558 siblings (Figure 13G). The immunostaining result of zrf-1 labeled gfap showed that cdnf mutant fish 559 revealed significantly less extensive radial glial fibers in the lateral region of hindbrain than their WT 560 siblings (Figure 13H and 13I).



# 561 Discussion

562 Despite the apparently typical general development and superficially normal behavior, zebrafish lacking 563 CDNF displayed hyperactivity and impairments in anxiety-related behavior, social preference, and shoal 564 cohesion. Reduction of proliferating cells, neural progenitor markers and radial glial cells in cdnf mutant 565 larvae brain may cause abnormal neurogenesis consequently leading to brain dysfunction at later stages. 566 Decreased sociability and increased seizure susceptibility were associated with deficiencies in several 567 neurotransmitter systems, including dopaminergic, GABAergic, and histaminergic neurons. Notably, there 568 was no overall difference in whole-brain dopamine levels, but a detailed examination of the two major 569 dopaminergic systems showed significant abnormalities in *cdnf* KO fish. A recent study on cdnf-/- mice 570 reports normal levels of brain dopamine and number of nigral dopamine neurons (Lindahl et al., 2020). Our 571 findings lend support to the hypothesis that CDNF acts as a general modulator that regulates neurogenesis and maturation of transmitter-specific neuronal types during development and throughout adulthood, 572 573 rather than a regulator of only dopaminergic systems. This concept is supported by the expression pattern 574 of cdnf mRNA during development and in the mature brain: it is detected in the anteroposterior axis of the 575 ventricular zones where neurogenesis actively happens from embryonal to adult zebrafish brain (Zupanc et 576 al., 2005; Kizil and Brand, 2011; Schmidt et al., 2013).

577

There is evidence that the unfolded protein response (UPR), which is essential in the mechanisms of MANF and CDNF, is associated with the generation and maturation of CNS neurons and circuits. MANF/Armet is upregulated in various forms of ER stress (Apostolou et al., 2008). ATF6 is a transcription factor activated as one component of the ER stress cascade, and its conditional activation induces MANF/Armet in cardiomyocytes (Tadimalla et al., 2008). In addition to ATF6 activation, the UPR cascade consists of activation of inositol-requiring enzyme 6 (Ire-6) and protein kinase (PKR)-like ER kinase (Perk) and is essential in nervous system development. Additionally, it supports the generation, maturation, and



585	maintenance of CNS neurons (Godin et al., 2016; Hetz and Saxena, 2017). For example, lack of functional
586	BiP/GRP78 – an essential component of the UPR – disturbs development of thalamocortical connections in
587	mice (Favero et al., 2013). Moreover, downregulation of the UPR alters generation of progenitor cells and
588	cell fate acquisition in the developing cerebral cortex (Laguesse et al., 2015). In agreement with the
589	structural similarities of MANF and CDNF (Lindahl et al., 2017), CDNF is also activated in the UPR.
590	Expression of CDNF in HEK293-T cells and hippocampal neurons activates the UPR during thapsigargin-
591	induced ER stress in both cell types, and attenuates expression of ER stress activated by the apoptotic
592	proteins CHOP and cleaved caspase 3 (Arancibia et al., 2018). There is clear evidence that exogenously
593	administered CDNF is also neuroprotective (Lindholm et al., 2007; Voutilainen et al., 2015). Indeed,
594	intrastriatally infused CDNF is taken up by neurons and transported retrogradely to, for example, the cortex
595	and substantia nigra in rats, and localized in endosomes rather than the ER (Matlik et al., 2017). Although a
596	cell surface receptor-mediated mechanism for secreted CDNF could be expected, no such mechanism has
597	yet been identified. Moreover, all observed abnormalities are not necessarily direct consequences of a
598	lack of CDNF, but may be secondary to the primary effects of the knockout, e.g. alterations in the
599	GABAergic or dopaminergic systems, which are known to regulate neurogenesis and differentiation (Saito
600	et al., 2010; Kim and Yoon, 2017).
601	Using the <i>cdnf</i> null mutant fish generated in this study, we first provide evidence that CDNF plays an

602 important role in the regulation of developing neurotransmitter circuits, including dopaminergic,

- 603 GABAergic, and histaminergic systems. Moreover, the increased seizure susceptibility revealed by PTZ
- administration in adult cdnf KO fish may be associated with the deficiency of the GABAergic and
- 605 glutamatergic systems in *cdnf* KO fish. As a consequence of this lack of functional *cdnf*, the dysregulated
- 606 homeostasis of the neurotransmitter connectivity leads to the impairment of social behaviors.

607

608 Loss of cdnf causes a dynamic alteration of dopaminergic systems in the brain



610 2005) complimentarily expressed in the brain (Chen et al., 2009; Filippi et al., 2010; Yamamoto et al., 2010) 611 are found in the zebrafish. In our cdnf KO mutant, the number of TH1 neurons was reduced in the prethalamus area, whereas an increased number of TH2-containing cells (teleost specific paralogous th) 612 appeared in the hypothalamic region. The zebrafish TH1 cell population in the prethalamus is homologous 613 614 to the mammalian DA population A13 in the zona incerta of the thalamus (Tay et al., 2011), which is more 615 susceptible to neurotoxic MPTP and MPP+ injury in the zebrafish brain (Sallinen et al., 2009). The 616 hypothalamic TH1 groups correspond to A12 and A14 DA groups in the arcuate and periventricular nucleus 617 of the hypothalamus (Tay et al., 2011), respectively. In the L1CAM (neural cell adhesion molecule L1) null 618 mice, abnormal distribution of dopaminergic neurons was evident in A12, A13 and A14 DA groups – but not 619 the A9 group - in the substantia nigra (Demyanenko et al., 2001). It has remained unclear whether cdnf 620 binds to potential signaling receptors to trigger downstream signal pathways. Alternatively, it is possible 621 that in the zebrafish brain, cdnf serves as a survival-promoting factor affecting the expression of essential 622 regulators that could regulate the number of TH1 dopaminergic neurons but negatively control the TH2-623 containing cell numbers in a regional-specific fashion. Finally, we cannot exclude the possibility that loss of 624 cdnf per se may induce unpredicted endoplasmic reticulum stress, oxidative stress or chronic inflammation, 625 which could result in neurodegeneration in other more vulnerable dopaminergic populations (Sprenkle et 626 al., 2017).

Due to the genome duplication in teleost fish (Postlethwait et al., 2004), two TH genes (Candy and Collet,

627

609

## 628 Impaired GABAergic and histaminergic system

It is evident that most of the dopaminergic neurons contain GABA as a co-transmitter in the preoptic area,
prethalamus, and hypothalamus regions (Filippi et al., 2014). Histamine neurons also contain GABA in all
vertebrates studied thus far (Airaksinen et al., 1992), including zebrafish (Sundvik and Panula, 2012).
Moreover, we have reported that dopaminergic signaling plays a crucial role in the specification of



633 hypothalamic neurotransmitter identity (Chen et al., 2016). The number of histaminergic neurons is 634 determined at least in part by dopamine produced by th2-expressing dopaminergic neurons in zebrafish 635 (Chen et al., 2016). The number of histaminergic neurons shows life-long plasticity in adult zebrafish through a Notch1 pathway regulated by presenilin 1 in the gamma-secretase complex (Sundvik et al., 636 637 2013). Dopamine activation also has a direct impact on GABAergic neuron development in zebrafish larvae 638 (Souza et al., 2011). Consequently, a decreased number of GABA-containing cells and histaminergic 639 neurons found in the hypothalamic area may also be caused by the dynamic alteration of dopaminergic 640 systems, specifically the increased expression of th2 in the hypothalamus, caused by a lack of cdnf. 641 Nevertheless, the wide distribution of abnormal cell populations in cdnf-deficient zebrafish is more likely to 642 derive from a direct effect on early neuronal proliferation, maturation, and transmitter specification.

643

# 644 Neurotransmitter systems associated with abnormal social behaviors

645 The neurotransmitter phenotype in the developing and mature nervous system is regulated by genetic and 646 environmental cues, in order to compensate for the changing homeostatic requirements and to maintain 647 the appropriate neuronal circuits during development in nervous system function (Dulcis et al., 2013; Dulcis 648 et al., 2017). Proper social responses require coordinated neurotransmitter circuits in the CNS. Dysfunction 649 of any main transmitter system is known to cause mental disorders and neurodegenerative diseases (Ng et al., 2015). The behavioral phenotype of the cdnf KO zebrafish is reminiscent of many neurological and 650 psychiatric conditions, such as attention deficit disorder, autism spectrum disorder, schizophrenia, or 651 652 epilepsy. The observed sensitivity to pentylenetetrazole-induced seizures may depend on an abnormal 653 GABAergic system and low expression of vGAT, since PTZ acts through the GABA-A receptors (Saito et al., 654 2010; Kim and Yoon, 2017). The abnormal histaminergic system may be responsible for the low level of 655 anxiety-related behavior observed in our novel tank test, since reducing histamine levels in the adult 656 zebrafish brain by prohibiting the hdc inhibitor alpha-fluoromethylhistidine has the same effect (Peitsaro et



al., 2003). The decrease in *hdc* expression and number of histamine-containing posterior hypothalamic neurons found in this study may be a direct result of lack of CDNF, or a secondary effect of the increased production of dopamine by the *th2*-expressing neurons in the same cluster of cells (Chen et al., 2016).

660

657

658

659

661 Taken together, this study highlights the novel and broad role of CDNF in shaping the neurotransmitter 662 circuits in the zebrafish brain, and provides evidence that cdnf has an impact on regulation of neural 663 progenitors and maintenance of neurotransmitter properties. Although the cdnf KO fish are superficially 664 normal, the altered transmitter networks produce a range of abnormal behaviors that resemble some 665 human neuropsychiatric conditions, including schizophrenia. Indeed, one study has already shown an 666 association between one SNP/haplotype in the human cdnf gene and schizophrenia characterized by 667 negative symptoms in the Han Chinese population (Yang et al., 2018). Interestingly, ER quality control of 668 protein processing is known to be associated with schizophrenia (Kim et al., 2019).

669

# 670 Author contributions

- 672 YCC designed the study, conducted and performed experiments, interpreted data and wrote the
- 673 manuscript. DB and SS performed experiments, acquired data and assisted in preparation of the
- 674 manuscript. SA provided vGAT materials. PP conceived and designed the study and wrote the manuscript.



#### Acknowledgements 675

This study was supported by grants from the Jane and Aatos Erkko Foundation, Sigrid Juselius Foundation, 676 677 Magnus Ehrnrooth's Foundation and Finska Läkaresällskapet. We thank Mr. Henri Koivula (BSc), Ms Riikka 678 Pesonen (BSc), and Ms. Noora Hellen (MSc) for expert technical help. We thank Dr. Mart Saarma, Dr. Esa 679 Korpi and Dr. Marnie Halpern for constructive comments on the manuscript. Zebrafish experiments were 680 carried out at the Zebrafish Unit of HiLife Infrastructures of the University of Helsinki funded in part by 681 Biocenter Finland.



"{ / Made Will Pdf Office

#### References 607

	082	Kelefences
<b>-</b>	683 684	Airaksinen MS, Alanen S, Szabat E, Visser TJ, Panula P (1992) Multiple neurotransmitters in the tuberomammillary nucleus: comparison of rat, mouse, and guinea pig. J Comp Neurol 323:103-116.
crip	685 686 687	Airavaara M, Harvey BK, Voutilainen MH, Shen H, Chou J, Lindholm P, Lindahl M, Tuominen RK, Saarma M, Hoffer B, Wang Y (2012) CDNF protects the nigrostriatal dopamine system and promotes recovery after MPTP treatment in mice. Cell Transplant 21:1213-1223.
ISO	688 689	Apostolou A, Shen Y, Liang Y, Luo J, Fang S (2008) Armet, a UPR-upregulated protein, inhibits cell proliferation and ER stress-induced cell death. Exp Cell Res 314:2454-2467.
osci Accepted Manuscript	690 691 692	Arancibia D, Zamorano P, Andres ME (2018) CDNF induces the adaptive unfolded protein response and attenuates endoplasmic reticulum stress-induced cell death. Biochim Biophys Acta Mol Cell Res 1865:1579-1589.
Z	693 694 695	Baronio D, Puttonen HAJ, Sundvik M, Semenova S, Lehtonen E, Panula P (2018) Embryonic exposure to valproic acid affects the histaminergic system and the social behaviour of adult zebrafish (Danio rerio). Br J Pharmacol 175:797-809.
teo	696 697	Benjamini Y, Krieger, A. M. & Yekutieli, D. (2006) Adaptive linear step-up procedures that control the false discovery rate. Biometrika 93:17.
0 D	698 699	Cachat J et al. (2010) Measuring behavioral and endocrine responses to novelty stress in adult zebrafish. Nat Protoc 5:1786-1799.
Ŭ	700	Candy J, Collet C (2005) Two tyrosine hydroxylase genes in teleosts. Biochim Biophys Acta 1727:35-44.
Ŭ V	701 702	Chao MV (2003) Neurotrophins and their receptors: a convergence point for many signalling pathways. Nat Rev Neurosci 4:299-309.
Ci /	703 704	Chao MV, Rajagopal R, Lee FS (2006) Neurotrophin signalling in health and disease. Clin Sci (Lond) 110:167- 173.
)S(	705 706	Chen YC, Priyadarshini M, Panula P (2009) Complementary developmental expression of the two tyrosine hydroxylase transcripts in zebrafish. Histochem Cell Biol 132:375-381.
	707 708	Chen YC, Sundvik M, Rozov S, Priyadarshini M, Panula P (2012) MANF regulates dopaminergic neuron development in larval zebrafish. Dev Biol 370:237-249.
JNeul	709 710 711	Chen YC, Semenova S, Rozov S, Sundvik M, Bonkowsky JL, Panula P (2016) A Novel Developmental Role for Dopaminergic Signaling to Specify Hypothalamic Neurotransmitter Identity. J Biol Chem 291:21880- 21892.
	712 713	Demyanenko GP, Shibata Y, Maness PF (2001) Altered distribution of dopaminergic neurons in the brain of L1 null mice. Brain Res Dev Brain Res 126:21-30.

GP, Shibata Y, Maness PF (2001) Altered distribution of dopaminergic neurons in the brain of



714 715	Dulcis D, Jamshidi P, Leutgeb S, Spitzer NC (2013) Neurotransmitter switching in the adult brain regulates behavior. Science 340:449-453.
716 717	Dulcis D, Lippi G, Stark CJ, Do LH, Berg DK, Spitzer NC (2017) Neurotransmitter Switching Regulated by miRNAs Controls Changes in Social Preference. Neuron 95:1319-1333 e1315.
718 719	Duy PQ, Berberoglu MA, Beattie CE, Hall CW (2017) Cellular responses to recurrent pentylenetetrazole- induced seizures in the adult zebrafish brain. Neuroscience 349:118-127.
720 721	Elfarnawany MH (2015) Signal Processing Methods for Quantitative Power Doppler Microvascular Angiography. In. Electronic Thesis and Dissertation Repository. 3106.
722 723 724	Favero CB, Henshaw RN, Grimsley-Myers CM, Shrestha A, Beier DR, Dwyer ND (2013) Mutation of the BiP/GRP78 gene causes axon outgrowth and fasciculation defects in the thalamocortical connections of the mammalian forebrain. J Comp Neurol 521:677-696.
725 726 727	Filippi A, Mueller T, Driever W (2014) vglut2 and gad expression reveal distinct patterns of dual GABAergic versus glutamatergic cotransmitter phenotypes of dopaminergic and noradrenergic neurons in the zebrafish brain. J Comp Neurol 522:2019-2037.
728 729 730	Filippi A, Mahler J, Schweitzer J, Driever W (2010) Expression of the paralogous tyrosine hydroxylase encoding genes th1 and th2 reveals the full complement of dopaminergic and noradrenergic neurons in zebrafish larval and juvenile brain. J Comp Neurol 518:423-438.
731 732	Finney JL, Robertson GN, McGee CA, Smith FM, Croll RP (2006) Structure and autonomic innervation of the swim bladder in the zebrafish (Danio rerio). J Comp Neurol 495:587-606.
733 734	Godin JD, Creppe C, Laguesse S, Nguyen L (2016) Emerging Roles for the Unfolded Protein Response in the Developing Nervous System. Trends Neurosci 39:394-404.
735 736 737	Green J, Collins C, Kyzar EJ, Pham M, Roth A, Gaikwad S, Cachat J, Stewart AM, Landsman S, Grieco F, Tegelenbosch R, Noldus LP, Kalueff AV (2012) Automated high-throughput neurophenotyping of zebrafish social behavior. J Neurosci Methods 210:266-271.
738 739	Hetz C, Saxena S (2017) ER stress and the unfolded protein response in neurodegeneration. Nat Rev Neurol 13:477-491.
740 741 742	Huang RQ, Bell-Horner CL, Dibas MI, Covey DF, Drewe JA, Dillon GH (2001) Pentylenetetrazole-induced inhibition of recombinant gamma-aminobutyric acid type A (GABA(A)) receptors: mechanism and site of action. J Pharmacol Exp Ther 298:986-995.
743 744	Hwang WY, Fu Y, Reyon D, Maeder ML, Tsai SQ, Sander JD, Peterson RT, Yeh JR, Joung JK (2013) Efficient genome editing in zebrafish using a CRISPR-Cas system. Nat Biotechnol 31:227-229.
745	Jones BE (2019) Arousal and sleep circuits. Neuropsychopharmacology.
746 747	Karhunen T, Airaksinen MS, Tuomisto L, Panula P (1993) Neurotransmitters in the nervous system of Macoma balthica (Bivalvia). J Comp Neurol 334:477-488.



748 749	Kaslin J, Panula P (2001) Comparative anatomy of the histaminergic and other aminergic systems in zebrafish (Danio rerio). J Comp Neurol 440:342-377.
750 751	Kelley LA, Mezulis S, Yates CM, Wass MN, Sternberg MJ (2015) The Phyre2 web portal for protein modeling, prediction and analysis. Nat Protoc 10:845-858.
752	Kemppainen S, Lindholm P, Galli E, Lahtinen HM, Koivisto H, Hamalainen E, Saarma M, Tanila H (2015)
753	Cerebral dopamine neurotrophic factor improves long-term memory in APP/PS1 transgenic mice
754	modeling Alzheimer's disease as well as in wild-type mice. Behav Brain Res 291:1-11.
755	Kim P, Scott MR, Meador-Woodruff JH (2019) Abnormal ER quality control of neural GPI-anchored proteins
756	via dysfunction in ER export processing in the frontal cortex of elderly subjects with schizophrenia.
757	Transl Psychiatry 9:6.
758	Kim YS, Yoon BE (2017) Altered GABAergic Signaling in Brain Disease at Various Stages of Life. Exp
759	Neurobiol 26:122-131.
760 761	Kimmel CB, Ballard WW, Kimmel SR, Ullmann B, Schilling TF (1995) Stages of embryonic development of the zebrafish. Dev Dyn 203:253-310.
762 763	Kizil C, Brand M (2011) Cerebroventricular microinjection (CVMI) into adult zebrafish brain is an efficient misexpression method for forebrain ventricular cells. PLoS One 6:e27395.
764	Kukko-Lukjanov TK, Panula P (2003) Subcellular distribution of histamine, GABA and galanin in
765	tuberomamillary neurons in vitro. J Chem Neuroanat 25:279-292.
766	Kysil EV, Meshalkina DA, Frick EE, Echevarria DJ, Rosemberg DB, Maximino C, Lima MG, Abreu MS,
767	Giacomini AC, Barcellos LJG, Song C, Kalueff AV (2017) Comparative Analyses of Zebrafish Anxiety-
768	Like Behavior Using Conflict-Based Novelty Tests. Zebrafish 14:197-208.
769	Laguesse S, Creppe C, Nedialkova DD, Prevot PP, Borgs L, Huysseune S, Franco B, Duysens G, Krusy N, Lee G,
770	Thelen N, Thiry M, Close P, Chariot A, Malgrange B, Leidel SA, Godin JD, Nguyen L (2015) A Dynamic
771	Unfolded Protein Response Contributes to the Control of Cortical Neurogenesis. Dev Cell 35:553-
772	567.
773 774	Laruelle M (2014) Schizophrenia: from dopaminergic to glutamatergic interventions. Curr Opin Pharmacol 14:97-102.
775	Latge C, Cabral KM, Almeida MS, Foguel D (2013) (1)H-, (13)C- and (15)N-NMR assignment of the N-
776	terminal domain of human cerebral dopamine neurotrophic factor (CDNF). Biomol NMR Assign
777	7:101-103.
778	Latge C, Cabral KM, de Oliveira GA, Raymundo DP, Freitas JA, Johanson L, Romao LF, Palhano FL, Herrmann
779	T, Almeida MS, Foguel D (2015) The Solution Structure and Dynamics of Full-length Human Cerebral
780	Dopamine Neurotrophic Factor and Its Neuroprotective Role against alpha-Synuclein Oligomers. J
781	Biol Chem 290:20527-20540.



782 783	Lindahl M, Saarma M, Lindholm P (2017) Unconventional neurotrophic factors CDNF and MANF: Structure, physiological functions and therapeutic potential. Neurobiol Dis 97:90-102.
784	Lindahl M, Chalazonitis A, Palm E, Pakarinen E, Danilova T, Pham TD, Setlik W, Rao M, Voikar V, Huotari J,
785	Kopra J, Andressoo JO, Piepponen PT, Airavaara M, Panhelainen A, Gershon MD, Saarma M (2020)
786	Cerebral dopamine neurotrophic factor-deficiency leads to degeneration of enteric neurons and
787	altered brain dopamine neuronal function in mice. Neurobiol Dis 134:104696.
788	Lindholm D, Makela J, Di Liberto V, Mudo G, Belluardo N, Eriksson O, Saarma M (2016) Current disease
789	modifying approaches to treat Parkinson's disease. Cell Mol Life Sci 73:1365-1379.
790	Lindholm P, Voutilainen MH, Lauren J, Peranen J, Leppanen VM, Andressoo JO, Lindahl M, Janhunen S,
791	Kalkkinen N, Timmusk T, Tuominen RK, Saarma M (2007) Novel neurotrophic factor CDNF protects
792	and rescues midbrain dopamine neurons in vivo. Nature 448:73-77.
793 794 795	Lindsey BW, Smith FM, Croll RP (2010) From inflation to flotation: contribution of the swimbladder to whole-body density and swimming depth during development of the zebrafish (Danio rerio). Zebrafish 7:85-96.
796	Liu H, Tang X, Gong L (2015) Mesencephalic astrocyte-derived neurotrophic factor and cerebral dopamine
797	neurotrophic factor: New endoplasmic reticulum stress response proteins. Eur J Pharmacol
798	750:118-122.
799 800	Livak KJ, Schmittgen TD (2001) Analysis of relative gene expression data using real-time quantitative PCR and the 2(-Delta Delta C(T)) Method. Methods 25:402-408.
801	Matlik K, Vihinen H, Bienemann A, Palgi J, Voutilainen MH, Booms S, Lindahl M, Jokitalo E, Saarma M,
802	Huttunen HJ, Airavaara M, Arumae U (2017) Intrastriatally Infused Exogenous CDNF Is Endocytosed
803	and Retrogradely Transported to Substantia Nigra. eNeuro 4.
804	Miller NY, Gerlai R (2011) Shoaling in zebrafish: what we don't know. Rev Neurosci 22:17-25.
805 806	Mitre M, Mariga A, Chao MV (2017) Neurotrophin signalling: novel insights into mechanisms and pathophysiology. Clin Sci (Lond) 131:13-23.
807	Mussulini BH, Leite CE, Zenki KC, Moro L, Baggio S, Rico EP, Rosemberg DB, Dias RD, Souza TM, Calcagnotto
808	ME, Campos MM, Battastini AM, de Oliveira DL (2013) Seizures induced by pentylenetetrazole in
809	the adult zebrafish: a detailed behavioral characterization. PLoS One 8:e54515.
810	Nasrolahi A, Mahmoudi J, Akbarzadeh A, Karimipour M, Sadigh-Eteghad S, Salehi R, Farhoudi M (2018)
811	Neurotrophic factors hold promise for the future of Parkinson's disease treatment: is there a light
812	at the end of the tunnel? Rev Neurosci 29:475-489.
813 814	Ng J, Papandreou A, Heales SJ, Kurian MA (2015) Monoamine neurotransmitter disordersclinical advances and future perspectives. Nat Rev Neurol 11:567-584.
815 816	Panula P, Airaksinen MS, Pirvola U, Kotilainen E (1990) A histamine-containing neuronal system in human brain. Neuroscience 34:127-132.



817 818 819	Parkash V, Lindholm P, Peranen J, Kalkkinen N, Oksanen E, Saarma M, Leppanen VM, Goldman A (2009) The structure of the conserved neurotrophic factors MANF and CDNF explains why they are bifunctional. Protein Eng Des Sel 22:233-241.
820 821	Peitsaro N, Kaslin J, Anichtchik OV, Panula P (2003) Modulation of the histaminergic system and behaviour by alpha-fluoromethylhistidine in zebrafish. J Neurochem 86:432-441.
822 823	Postlethwait J, Amores A, Cresko W, Singer A, Yan YL (2004) Subfunction partitioning, the teleost radiation and the annotation of the human genome. Trends Genet 20:481-490.
824 825	Provensi G, Costa A, Izquierdo I, Blandina P, Passani MB (2018) Brain histamine modulates recognition memory: possible implications in major cognitive disorders. Br J Pharmacol.
826 827 828	Puttonen HAJ, Sundvik M, Semenova S, Shirai Y, Chen YC, Panula P (2018) Knockout of histamine receptor H3 alters adaptation to sudden darkness and monoamine levels in the zebrafish. Acta Physiol (Oxf) 222.
829 830 831	Ren X, Zhang T, Gong X, Hu G, Ding W, Wang X (2013) AAV2-mediated striatum delivery of human CDNF prevents the deterioration of midbrain dopamine neurons in a 6-hydroxydopamine induced parkinsonian rat model. Exp Neurol 248:148-156.
832 833 834 835	Saito K, Kakizaki T, Hayashi R, Nishimaru H, Furukawa T, Nakazato Y, Takamori S, Ebihara S, Uematsu M, Mishina M, Miyazaki J, Yokoyama M, Konishi S, Inoue K, Fukuda A, Fukumoto M, Nakamura K, Obata K, Yanagawa Y (2010) The physiological roles of vesicular GABA transporter during embryonic development: a study using knockout mice. Mol Brain 3:40.
836 837	Sallinen V, Torkko V, Sundvik M, Reenila I, Khrustalyov D, Kaslin J, Panula P (2009) MPTP and MPP+ target specific aminergic cell populations in larval zebrafish. J Neurochem 108:719-731.
838	Schmidt R, Strahle U, Scholpp S (2013) Neurogenesis in zebrafish - from embryo to adult. Neural Dev 8:3.
839 840	Semenova SA, Chen YC, Zhao X, Rauvala H, Panula P (2014) The tyrosine hydroxylase 2 (TH2) system in zebrafish brain and stress activation of hypothalamic cells. Histochem Cell Biol 142:619-633.
841 842	Sousa-Victor P, Jasper H, Neves J (2018) Trophic Factors in Inflammation and Regeneration: The Role of MANF and CDNF. Front Physiol 9:1629.
843 844 845	Souza BR, Romano-Silva MA, Tropepe V (2011) Dopamine D2 receptor activity modulates Akt signaling and alters GABAergic neuron development and motor behavior in zebrafish larvae. J Neurosci 31:5512- 5525.
846 847	Sprenkle NT, Sims SG, Sanchez CL, Meares GP (2017) Endoplasmic reticulum stress and inflammation in the central nervous system. Mol Neurodegener 12:42.
848 849	Sundvik M, Panula P (2012) Organization of the histaminergic system in adult zebrafish (Danio rerio) brain: neuron number, location, and cotransmitters. J Comp Neurol 520:3827-3845.



850 851	Sundvik M, Chen YC, Panula P (2013) Presenilin1 regulates histamine neuron development and behavior in zebrafish, danio rerio. J Neurosci 33:1589-1597.
852 853 854	Sundvik M, Kudo H, Toivonen P, Rozov S, Chen YC, Panula P (2011) The histaminergic system regulates wakefulness and orexin/hypocretin neuron development via histamine receptor H1 in zebrafish. FASEB J 25:4338-4347.
855 856 857	Tadimalla A, Belmont PJ, Thuerauf DJ, Glassy MS, Martindale JJ, Gude N, Sussman MA, Glembotski CC (2008) Mesencephalic astrocyte-derived neurotrophic factor is an ischemia-inducible secreted endoplasmic reticulum stress response protein in the heart. Circ Res 103:1249-1258.
858 859 860	Tay TL, Ronneberger O, Ryu S, Nitschke R, Driever W (2011) Comprehensive catecholaminergic projectome analysis reveals single-neuron integration of zebrafish ascending and descending dopaminergic systems. Nat Commun 2:171.
861 862	Thisse C, Thisse B (2008) High-resolution in situ hybridization to whole-mount zebrafish embryos. Nat Protoc 3:59-69.
863 864 865	Voutilainen MH, Arumae U, Airavaara M, Saarma M (2015) Therapeutic potential of the endoplasmic reticulum located and secreted CDNF/MANF family of neurotrophic factors in Parkinson's disease. FEBS Lett 589:3739-3748.
866 867 868	Voutilainen MH, Back S, Peranen J, Lindholm P, Raasmaja A, Mannisto PT, Saarma M, Tuominen RK (2011) Chronic infusion of CDNF prevents 6-OHDA-induced deficits in a rat model of Parkinson's disease. Exp Neurol 228:99-108.
869 870 871	Yamamoto K, Ruuskanen JO, Wullimann MF, Vernier P (2010) Two tyrosine hydroxylase genes in vertebrates New dopaminergic territories revealed in the zebrafish brain. Mol Cell Neurosci 43:394-402.
872 873	Yan Y, Rato C, Rohland L, Preissler S, Ron D (2019) MANF antagonizes nucleotide exchange by the endoplasmic reticulum chaperone BiP. Nat Commun 10:541.
874 875 876	Yang Y, Yu H, Li W, Liu B, Zhang H, Ding S, Lu Y, Jiang T, Lv L (2018) Association between cerebral dopamine neurotrophic factor (CDNF) 2 polymorphisms and schizophrenia susceptibility and symptoms in the Han Chinese population. Behav Brain Funct 14:1.
877 878	Zhou C, Xiao C, Commissiong JW, Krnjevic K, Ye JH (2006) Mesencephalic astrocyte-derived neurotrophic factor enhances nigral gamma-aminobutyric acid release. Neuroreport 17:293-297.
879 880 881	Zhou W, Chang L, Fang Y, Du Z, Li Y, Song Y, Hao F, Lv L, Wu Y (2016) Cerebral dopamine neurotrophic factor alleviates Abeta25-35-induced endoplasmic reticulum stress and early synaptotoxicity in rat hippocampal cells. Neurosci Lett 633:40-46.
882 883	Zupanc GK, Hinsch K, Gage FH (2005) Proliferation, migration, neuronal differentiation, and long-term survival of new cells in the adult zebrafish brain. J Comp Neurol 488:290-319.



887	Figure 1. Predicted domain structures and spatiotemporal expression of zebrafish cdnf. (A) Secondary
888	structure, and (B) predictive 3D model of zebrafish cdnf by Phyre2 modeling with human CDNF. (C) whole-
889	mount in situ hybridization highlighting cdnf expression in the head, eyes, heart, muscles, and optic vesicles
890	during development. (D) Quantitative RT-PCR showing the zygotic <i>cdnf</i> mRNA expression at various
891	developmental stages (one-way ANOVA, F (6, 14) = 40.31, p<0.0001 n=3 ), and (E) in various male and
892	female adult organs (two-way ANOVA, F (1, 32) = 3.885,p=0.0574, n=4/group). Green helices indicate
893	alpha-helices, blue arrows indicate beta-strands. Grey lines indicate the conserved amino acid residues. G
894	indicates the 3-trun helix. T indicates hydrogen bonded turn. S indicates the bend. H, heart. HB, hindbrain.
895	ov, optic vesicle. Data are mean $\pm$ SEM; one-way or two-way ANOVA was used for statistics.

Figure 2. CRISPR/Cas9-generated *cdnf* mutant zebrafish. (A) Scheme of CRISPR/Cas9-generated 14-base
pair deletion in exon2 of *cdnf*. (B) Sequence chromatogram showing a premature stop codon of a
homozygous *cdnf* mutant zebrafish. (C) Results of the HRM analysis showing the distinctive melting curves
of each genotype. (D) Reduction in *cdnf* mRNA expression shown in the brains of 8-dpf and (E) 1-mpf *cdnf*mutant fish. (F) No obvious gross phenotype in larvae and adult *cdnf* mutant fish. PPa, anterior
parvocellular preoptic nucleus. PTv, ventral part of posterior tuberculum. T, midbrain tegmentum. TeO,
tectum opticum. Scale bar is 200µm in (D), 1mm (10 dpf ) and 1cm (10 mpf) in (F).

904

Figure 3. qPCR analysis of *cdnf* and neurotransmitter synthesis enzymes at larval, adulthood, and aging
stages. (A-C) Significant reduction of *cdnf* mRNA in *cdnf*-deficient (knock-out) fish (Unpaired t test, t=4.675,
df=22, two-tailed p=0.0001; t=4.245, df=8, p=0.0028; t=3.280, df=8, p=0.0112). (D-F) Significant increase of *th2* transcripts in *cdnf*-deficient fish (Unpaired t test, t=4.043, df=22, p= 0.0005; t=2.901, df=8, p= 0.0198;

t=5.450, df=8, p= 0.0006). (G-I) Non-significant differences in *th1* mRNA expression between groups (Unpaired t test, t=0.6318, df=22, p= 0.5340; t=1.024, df=8, p= 0.3358; t=0.7477, df=8, p= 0.4760). (J-L) Significant reduction of *hdc* mRNA expression in adult brains (Unpaired t test, t=0.052, df=22, p=0.9590; t=2.473, df=8, p=0.0385; t=1.042, df=8, p=0.3278). qPCR analysis relative to expression of the housekeeping

gene *rpl13a*; values are mean ± SEM. n=12/ group for 8-dpf fish, n=5/ group for 8-mpf brains, n=5/ group
for 18-mpf brains in each *cdnf* knock-out and wild-type group. Data are mean ± SEM. Student's *t*-test was
used for statistical analysis \*p<0.05, \*\*p<0.01, and \*\*\*p<0.001.</li>

916

909

910

911

912

917 Figure 4. Selective alteration in dopaminergic systems in cdnf mutant fish. (A) Co-labeling of zebrafish tyrosine hydroxylase 1 (th1) and tyrosine hydroxylase 2 (th2) of 8-dpf cdnf wild-type (WT) brains. (B) Co-918 919 labeling of zebrafish tyrosine hydroxylase 1 (th1) and tyrosine hydroxylase 2 (th2) of 8-dpf cdnf knock-out 920 (KO) brains. (C) Higher magnification images of TH2 10/10b (Hc) group, TH1 10 group, and TH1 5,6,11 group 921 of cdnf WT brains. (D) Higher magnification images of TH2 10/10b (Hc) group, TH1 10 group, and TH1 5,6,11 922 group of cdnf KO brains. (E) Significant increase in TH1/TH2 immunoreactive cell number in the caudal 923 hypothalamus area (Unpaired t test, t=3.398, df=14, p= 0.0043, n=8/group; Hc, 10/10b th population) in the 924 cdnf KO group. (F) No significant change in TH1 immunoreactive cell number in the caudal hypothalamus 925 area (Unpaired t test, t=0.9245, df=14, p= 0.3709, n=8/ group; Hc, 10 th population) in the cdnf KO group. 926 (G) Significant decrease in TH1-positive cell number in the prethalamus (Unpaired t test, t=4.472, df=16, 927 p=0.0004; n=8/ group, th1 group 5,6,11) in the cdnf KO group. (H) 5-HT immunoreactivity in 8-dpf WT larval 928 brains and cdnf KO larval brains (n=7). (I) No significant difference in 5HT immunoreactive cell numbers in 929 the caudal hypothalamus area (Unpaired t test, t=0.7817, df=12, p= 0.4495, n=7/ group) (J) in situ 930 hybridization results showing a higher intensity of th2 signals in th2 10b group (Hc, caudal hypothalamus) in 931 8-dpf cdnf KO fish (n=8). In particular, TH1+TH2 (rabbit anti-th1 and th2 antibody) recognized both 932 zebrafish th1 and th2 dopaminergic neurons. TH1 (mouse anti-tyrosine hydroxylase antibody) specifically



933 recognized zebrafish th1. 5-HT, rabbit anti-serotonin antibody. Data are mean ± SEM. Student's *t*-test was
934 used for statistical analysis. \*\*p<0.01, \*\*\*p<0.001. Scale bar is 100μm.</li>

935

936 Figure 5. Deficient proliferating cells and histaminergic neurons in cdnf mutant fish. (A) Co-labeling of 937 proliferation marker (EdU), anti-histamine immunoreactivity, anti-HuC immunoreactivity, and a merged 938 image of triple labeled stacks of an 8-dpf cdnf WT brain. (B) Triple labeling of an 8-dpf cdnf KO brain. (C) 939 Quantification of EdU-positive cell numbers, and higher magnification images of EdU-labeled cells in the 940 caudal hypothalamic area (Hc) (Unpaired t test, t=2.193, df=14, p=0.0457, n=8 cdnf WT, and n=8 cdnf KO 941 fish). (D) Quantification of fluorescence intensity of HuC immunoreactive cells, and higher magnification images of the caudal hypothalamus (Unpaired test, t=2.362, df=14, p=0.0332, n=8 cdnf WT, and n=8 cdnf 942 943 KO fish). (E) Quantification of histamine-positive cell numbers, and higher magnification images of 944 histamine immunostaining images (Unpaired t test, t=6.584, df=12, p<0.0001, n=7 cdnf WT, and n=7 cdnf 945 KO fish). (F) Quantification of histidine decarboxylase (hdc) mRNA-containing cell numbers (unpaired t test, 946 t=4.124, df=12, p=0.0014, n=6 cdnf wild-type, and n=8 cdnf KO fish). (G) Quantification of orexin-positive 947 cell numbers, and higher magnification images of orexin immunostaining images (Unpaired t test, t=2.683, 948 df=16, p= 0.0163, n=9 cdnf WT, and n=9 cdnf KO fish). (H) Significant decrease of sox2a transcripts in cdnf-949 deficient fish (Unpaired t test, t=2.614, df=12, p= 0.0226). Marked areas were used a regions of interest for 950 measurement of fluorescence intensity. Data are mean ± SEM. Student's t-test was used for statistical analysis. \*\*p<0.01, \*\*\*p<0.001. Scale bar is 100µm. 951

952

Figure 6. Selective impairment of GABAergic system in *cdnf* KO fish. (A) Co-labeling of anti-acetylated
tubulin (showing axons) and GABA with antibody (showing GABAergic cells) of 8-dpf *cdnf* WT brains. (B)
Double immunostaining of 8-dpf *cdnf* KO brains. (C) Quantification of GABA immunoreactive cell numbers



956	in the ventral part of the posterior tuberculum (PTv), and higher magnification images of GABA-labelled
957	cells (Unpaired t test, t=9.989, df=14, p <0.0001, n=8/group). (D) Quantification of GABA immunoreactive
958	cell numbers in the caudal hypothalamus (Hc), and higher magnification images of GABA-labelled cells
959	(Unpaired test, t=5.503, df=14, p <0.0001, n=8/group). (E) Quantification of fluorescence intensity of
960	acetylated tubulin immunoreactive projections, and higher magnification images of acetylated tubulin
961	immunoreactive projections (Unpaired t test, t=0.7879, df=14, p=0.4439, n=8/group). White rectangles and
962	arrows indicate a noteworthy reduction of GABA-staining cells in the PTv and Hc area, respectively. The
963	marked area was used as a region of interest for measurement of fluorescence intensity. Data are mean $\pm$
964	SEM. Student's <i>t</i> -test was used for statistical analysis. *** $p<0.001$ . Scale bar is 100 $\mu$ m.

966 Figure 7. slc32a/vGAT downregulation in cdnf KO fish. (A) Quantification of slc32a/vGAT mRNA 967 expression relative to the housekeeping gene rpl13a in 8-dpf fish (Unpaired t test, t=2.508, df=14, p= 968 0.0251, n=8/group). (B) In situ hybridization of vGAT mRNA expression of 8-dpf brains (n=5). (C) 969 Quantification of gad1b mRNA expression relative to rpl13a in 8-dpf fish (Unpaired t test, t=2.077, df=14, 970 p= 0.0567). (D) Quantification of gad2a mRNA expression relative to the rpl13a in 8-dpf fish (Unpaired t 971 test, t=2.508, df=14, p= 0.0251). (E) Quantification of vGlut2 mRNA expression relative to rpl13a in 8-dpf 972 fish (Unpaired t test, t=2.508, df=14, p= 0.0251). Arrows and red rectangles indicate downregulated 973 expression of vGAT in the hypothalamus (H), preoptic region (Po), ventral posterior tuberculum (PTv) and 974 ventral thalamus (VT). Data are mean ± SEM. Student's t-test was used for statistical analysis. \*p<0.05. 975 Scale bar is 100µm.

976

977 Figure 8. 8-dpf larval sleep-related behavior



978	(A) Locomotor activity under 14:10 (light:dark) illumination conditions (Multiple t tests using Two-stage
979	step-up method of Benjamini, Krieger and Yekutieli)(Benjamini, 2006). (B) Average cumulative duration (in
980	s) in 15 min time bins of movement during light conditions (Unpaired t test, t=2.304, df=62, p= 0.0246). (C)
981	Average cumulative duration of movement during the second treatment of light conditions in 15 min time
982	bins (Unpaired t test, t=2.151, df=12, p= 0.0525). (D) Duration of rest (not moving) during dark conditions in
983	15 min time bins (Unpaired t test, t=9.159, df=76, p <0.0001). (E) Average cumulative duration of
984	movement during dark conditions in 15 min time bins (Unpaired t test, t=9.159, df=76, p <0.0001). n=16/
985	group. Data are mean ± SEM. Student's <i>t</i> -test and one-way ANOVA analysis with multiple comparisons was
986	used for statistical analysis *p<0.05 and ***p<0.001.

Figure 9. Social preference deficiency in *cdnf* KO adult fish. (A) Schemes of visually mediated social
preference behavior setup and representative movement traces of *cdnf* WT and KO fish during 10 min
recording intervals. (B) Ratio of cumulative duration in the distal, object and stimulus/conspecific zone. (C)
Cumulative time spent in the stimulus (conspecific) zone. (Unpaired t test, t=2.357, df=28, p= 0.0257). (D)
Cumulative time spent in the object zone (Unpaired t test, t=1.156, df=28, p= 0.2575). (E) Cumulative time
spent in the distal zone (Unpaired t test, t=2.217, df=28, p= 0.0349). n=15/ group. Data are mean ± SEM.
Student's *t*-test was used for statistical analysis. \*p<0.05.</li>

995

Figure 10. Impaired bottom-dwelling behavior in *cdnf* KO adult fish. (A) Schemes of the novel tank test with three digitized zones and representative movement traces of *cdnf* WT and KO siblings during a 6 min recording period. (B) Ratio of cumulative duration in the top, middle and bottom zone. (C) Amount of time spent in the top zone (Unpaired t test, t=2.942, df=18, p= 0.0087). (D) Amount of time spent in the middle zone (Unpaired t test, t=0.01053, df=18, p= 0.9917). (E) Amount of time spent in the bottom zone (unpaired

44



1001 t test, t=3.029, df=18, p= 0.0072). (F) Average velocity during the 6 min video tracking period (Unpaired t 1002 test, t=1.253, df=18, p= 0.2261). (G) Vasculature by autofluorescence and TH1 immunostaining of the 1003 posterior chamber of the swim bladder in cdnf WT and cdnf KO fish. Inserts show images of dissected swim 1004 bladders. (H) Quantification of V3 volume of the posterior chamber (Unpaired t test, t=0.3488, df=6, p= 1005 0.7392). (I) Quantification of vascular length density of the posterior chamber (Unpaired t test, t=0.0646, 1006 df=6, p= 0.9506). (J) Quantification of TH fluorescence intensity of the posterior chamber (Unpaired t test, t=1.138, df=6, p= 0.2983). n=10 for WT and cdnf KO fish in the Novel tank analysis. n=4 for WT and cdnf KO 1007 1008 in the swim bladder analysis. Data are mean ± SEM. Student's *t*-test was used for statistical analysis. 1009 \*\*p<0.01. Scale bar is 100 μm.

1010

1011 Figure 11. Decreased shoal cohesion in cdnf KO adult fish. The upper panel shows the shoaling behavior 1012 test on 6-mpf male cdnf WT and KO fish (n=5 in each trial) during a 10 min video tracking period; four trials 1013 were analyzed. (A) Average velocity, in 1 min time bins (Multiple t tests, 1min, t=2.794, df=38.0 p= 0.0477; 1014 2min, t=3.576, df=38, p=0.0087; 3min, t=4.344, df=38, p= 0.001; 7min, t= 2.991, df=38, p=0.033; 10min, 1015 t=3.361, df=38.00, p=0.014). (B) Average velocity during the 10 min video tracking period (Unpaired t test, 1016 t=3.300, df=38, p= 0.0021). (C) Average inter-individual distance of total trials (Unpaired t test, t=4.964, 1017 df=78, p <0.0001). (D) Average time spent in the proximity (i.e. less than 2 cm) of the nearest neighbor. The 1018 lower panel shows the shoaling behavior test on 18-mpf male *cdnf* WT and KO fish (n=5 in each trial); three 1019 trials were analyzed (Unpaired t test, t=2.973, df=38, two-tailed p= 0.0051). (E) Average velocity, in 1 min 1020 time bins (Multiple t tests, 1min, t= 4.351, df=28.0 p= 0.0016; 2min, t= 3.898, df=28, p= 0.0050; 3min, t= 1021 3.726, df=28, p= 0.0070; 8min, t= 3.392, df=28, p= 0.0145). (F) Average velocity during the 10 min video 1022 tracking period (Unpaired t test, t=4.122, df=28, p= 0.0003). (G) Average inter-individual distance of total 1023 trials (Unpaired t test, t=7.264, df=58, p <0.0001). (H) Average time spent in the proximity of closest 1024 neighbor (Unpaired t test, t=1.649, df=28, p= 0.1103). Data are mean ± SEM. Student's t-test and one-way

45

🏏 Mado WAA Pd4 Office

ANOVA analysis with multiple comparisons was used for statistical analysis. \*p<0.05, \*\*p<0.01, and

1026 \*\*\*p<0.001.

1027

1025

1028	Figure 12. Increased seizure susceptibility in cdnf KO adult fish. (A) Scheme of the PTZ administration
1029	procedure. (B) Seizure scores after 5 min of PTZ exposure (Two-way ANOVA, F (2, 15) = 0.8333, P=0.4538;
1030	Multiple t test; Day1, t= 2.712, df=10, p= 0.0433; Day2, t= 2.712, df=10, p= 0.0433; Day3, t= 4.000, df=10,
1031	p= 0.0075). (C) Seizure onset latency to score of 4 (Two-way ANOVA, F (2, 30) = 2.973, P=0.0664; Multiple t
1032	tests; Day1, t= 1.265, df=10, p= 0.2344; Day2, t= 6.078, df=10, p= 0.0004; Day 3, t= 4.065, df=10, p=
1033	0.0045). (D) Duration of immobility during 5 min of PTZ exposure (Two-way ANOVA, F (2, 30) = 0.3478,
1034	P=0.7091; Multiple t tests; Day1, t= 0.4509, df=10, p= 0.6616; Day2, t= 1.853, df=10, p= 0.2554; Day 3, t=
1035	1.674, df=10, p= 0.2554). (E) Total distance travelled during 5 min of PTZ exposure (Two-way ANOVA, F (2,
1036	30) = 0.4349, P=0.6513; Multiple t tests; Day1, t= 1.053, df=10, p= 0.6168; Day2, t=1.158, df=10, p= 0.6168;
1037	Day 3, t= 0.0195, df=10, p=0.9848). n=6 in each group. Data are mean ± SEM. Two-way ANOVA analysis
1038	with multiple comparisons was used for statistical analysis. *p<0.05, **p<0.01, and ***p<0.001.

1039

1040	Figure 13. Results of qPCR analysis in PTZ-treated cdnf knock-out fish. Quantification of relative
1041	expression of ( <b>A</b> ) <i>cdnf</i> (Two-way ANOVA, F (1, 16) = 40.14, P<0.0001), ( <b>B</b> ) <i>manf</i> (Two-way ANOVA, F (1, 16)
1042	= 0.02213, P=0.8836), ( <b>C</b> ) <i>slc17a6a/vGlut2</i> (Two-way ANOVA, F (1, 16) = 16.16, P=0.0010), ( <b>D</b> ) <i>slc32a1/vGAT</i>
1043	(Two-way ANOVA, F (1, 16) = 40.14, P<0.0001), (E) gad2a/gad65 (Two-way ANOVA, F (1, 16) = 10.68,
1044	P=0.0048), (F) gad1b/gad67 (Two-way ANOVA, F (1, 16) = 4.052, P=0.0613), and (G) gfap (Two-way ANOVA,
1045	F (1, 16) = 8.813, P=0.0091) in 6-mpf brains with or without PTZ treatment. n=5 in each group. (H)
1046	Quantification of fluorescence intensity of zrf-1 immunostaining signals of 10-dpf cdnf wild-type and knock-
1047	out fish brains (Two-way ANOVA, F (1,24)= 33.8 P<0.0001). (I) Quantification of fluorescence intensity of

1049 RV, rhombencephalic ventricle; LR, lateral region of raphe. Data are mean ± SEM. Two-way ANOVA analysis with Tukey's multiple comparisons test was used for statistical analysis. \*p<0.05, \*\*p<0.01, and 1050 \*\*\*p<0.001. Scale bar is 100µm. 1051 1052 1053 Table 1 1054 List of primers used in this study 1055 1056 Table 2

gfap-positive radial glial cells (shown in panel H) was done in the regions of interest shown in white boxes.

1057 HPLC analysis results of monoamine concentrations of larvae, adult brains and aging brains





#### Table 1 List of primers used in this study

gene	Forward primer	Reverse primer	note	ACCESSION
actb1	CGAGCAGGAGATGGGAACC	CAACGGAAACGCTCATTGC	qPCR	NM_131031.1
cdnf	TGAAGTTCCCTTGGAAGTGCG	TGTGCAGATATTGCACATGGC	RT-PCR cloning	NM_001123281.1
cdnf	TTCTGCAGCCAAAGTGACCG	TCTGTGCTCCAGTCAAGAACC	qPCR	NM_001123281.1
cdnf	CACGAAATCAGCCCTCCAGT	GCTGAAGCCTCTGGCAGATT	crispr_cloning	BX901962.8
cdnf	TGTGTGTGGGGGTTTTTGGGA	GCCGATTCTCTTTCCCAGTAGTCTC	HRM	BX901962.8
cdnf	TAGGCCCTCCTCCACCAGCTCT	AAACAGAGCTGGTGGAGGAGGG	sgRNA cloning	NM_001123281.1
gad1b/67	GGCCAAGGGCACGATTGGGT	GCATGCCACGCAGACTCGGT	qPCR	NM_194419.1
gad2/65	GCGGAGGCATCGGCTCCAAA	GCCGCAGCTCTCGGCTGTAG	qPCR	NM_001017708.2
gfap	GAAGCAGGAGGCCAATGACTATC	GGACTCATTAGACCCACGGAGAG	qPCR	NM_131373.2
hdc	TTCATGCGTCCTCTCCTGC	CCCCAGGCATGATGATGTTC	qPCR	NM_001102593.1
manf	ACCATGTGCCAGTGGAAAAGA	TCGACGGAGCTCAAGTCAAC	qPCR	NM_001076629.1
rpl13a	AGAGAAAGCGCATGGTTGTCC	GCCTGGTACTTCCAGCCAACTT	qPCR	NM_212784.1
sox2a	CCTATTCGCAGCAAAGCACG	GGAATGAGACGACGACGTGA	qPCR	NM_213118.1
slc17a6a/vGlut2	CATCCTGTCTACAACTACGGTT	CCAACACCAGAAATGAAATAGCCA	qPCR	NM_001009982.1
slc32a1/vGAT	AATACGCGTCACCACGAGAG	GAGCTCGATGATCTGTGCCA	cloning	NM_001080701.1
slc32a1/vGAT	CGGACAAGCCCAGAATCACT	CGACGGCGGCGAATATAATG	qPCR	NM_001080701.3
th	GACGGAAGATGATCGGAGACA	CCGCCATGTTCCGATTTCT	qPCR	NM_131149.1
th2	CTCCAGAAGAGAATGCCACATG	ACGTTCACTCTCCAGCTGAGTG	qPCR	NM_001001829.1



Table 2 HPLC analysis of monoamine concentrations of larvae, adult brains and aging brains

	19-momth-old brain			8-momth-old brain			8-dpf (8 larvae per tube)		
pmole/mg protein	WT (n=5)	KO (n=5)	p value	WT (n=9)	KO (n=9)	p value	WT (n=3)	KO (n=3)	p value
Dopamine	22.39 ± 0.3935	21.14 ± 0.6298	0.13	16.52 ± 0.542	15.97 ± 0.433	0.4451	2.834 ± 0.1438	3.21 ± 0.2845	0.3041
Norepinephrine	58.79 ± 3.076	56.32 ± 2.85	0.5707	46.29 ± 1.956	43.3 ± 1.243	0.216	7.2 ± 0.1838	8.239 ± 0.56.	0.1528
DOPAC	4.699 ± 0.3663	3.506 ± 0.2053	0.0218	2.764 ± 0.1298	2.452 ± 0.2412	0.2713	1.721 ± 0.1544	1.605 ± 0.08641	0.549
Homovanillic acid	12.48 ± 1.131	8.847 ± 0.1623	0.013	17.54 ± 1.768	8.494 ± 1.607	0.0016	2.235 ± 0.007714	4.195 ± 1.205	0.1794
3-Methoxytyramine	1.539 ± 0.1343	1.343 ± 0.2165	0.4639	5.42 ± 0.6011	5.795 ± 0.438	0.6205	2.854 ± 0.1544	3.351 ± 0.4868	0.3855
Serotonin	23 ± 1.162	24.63 ± 0.6439	0.2543	16.83 ± 0.6696	19.43 ± 0.6398	0.0124	3.693 ± 0.157	3.902 ± 0.1672	0.4142
5-Hydroxyindoleacetic acid	19.81 ± 0.9596	13.7 ± 0.4645	0.0004	15.99 ± 0.8659	15.08 ± 1.173	0.5423	3.769 ± 0.03767	5.02 ± 0.6834	0.1416
Histamine	9.065 ± 0.4468	11.33 ± 1.745	0.244	5.958 ± 0.516	4.285 ± 0.3379	0.0154	7.805 ± 0.854	5.899 ± 1.09	0.2406

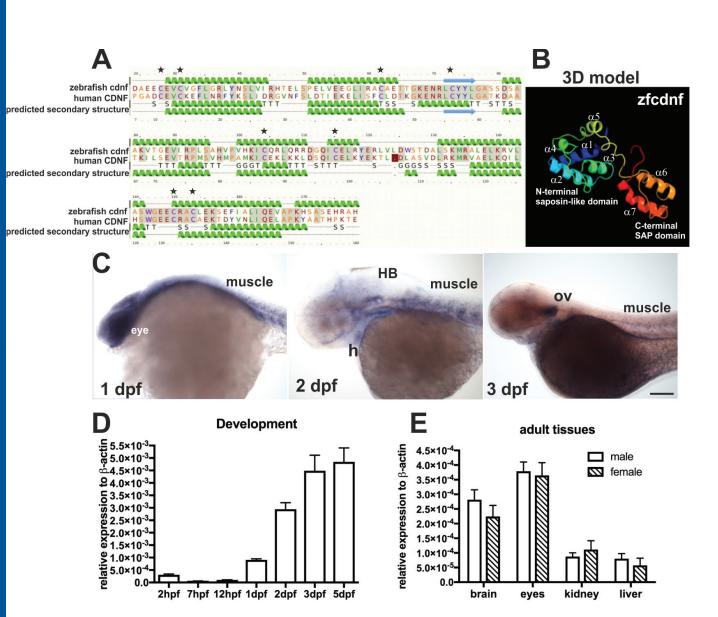
(A significant reduction in KO is indicated in red; a significant increase in KO is indicated in green. Data are mean ± SEM. Student's t-test was used for

2

statistical analysis)

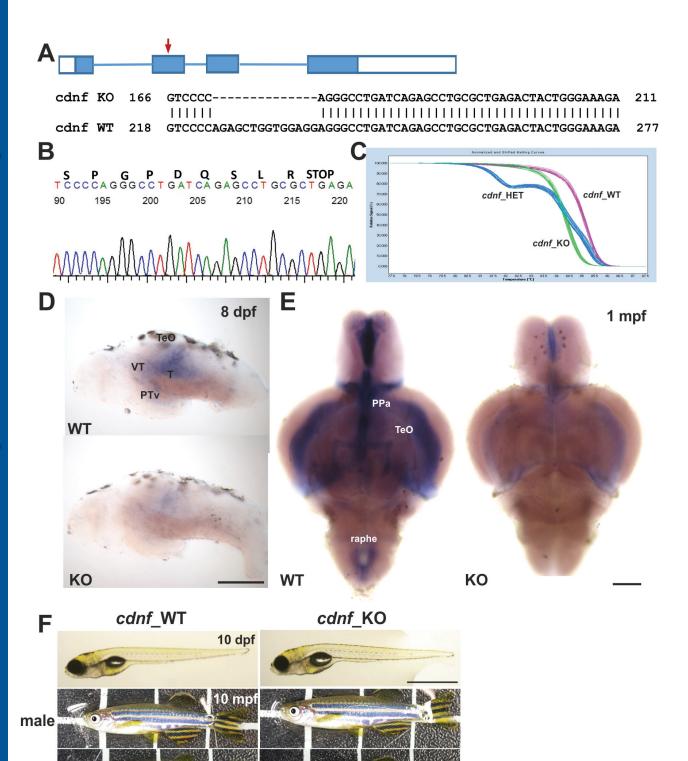




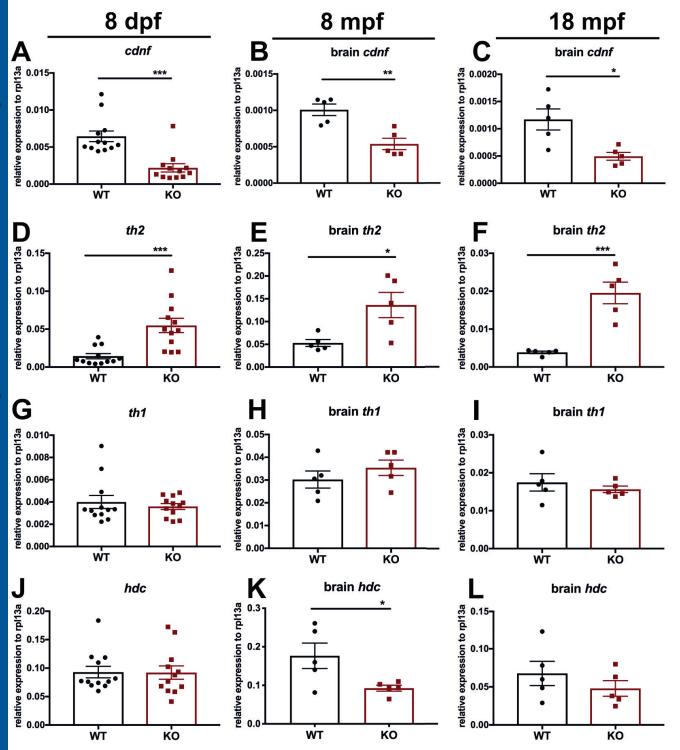


🏹 Made WAB Pdf Office

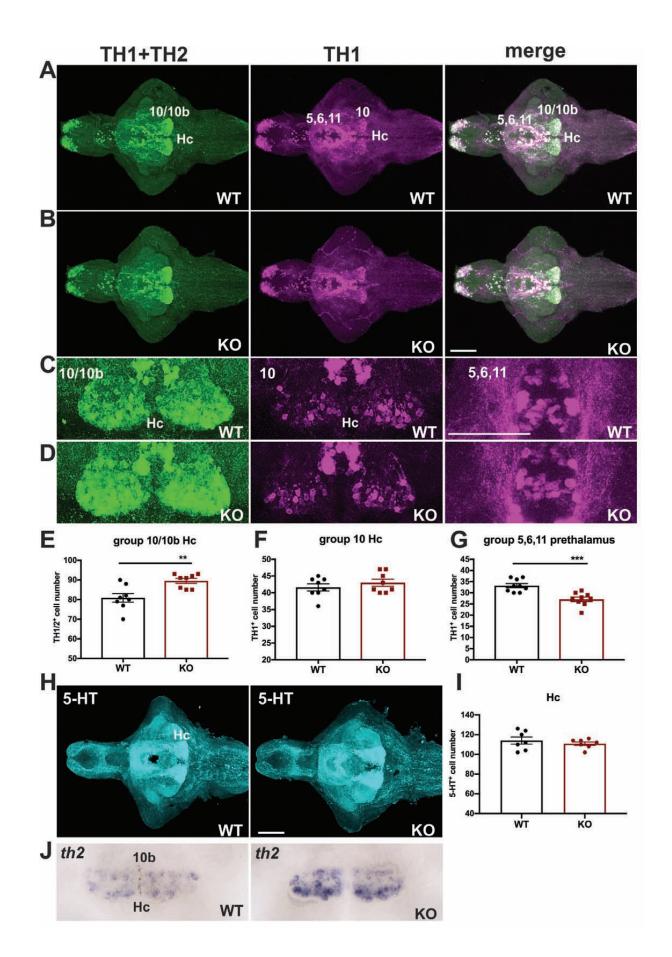
female





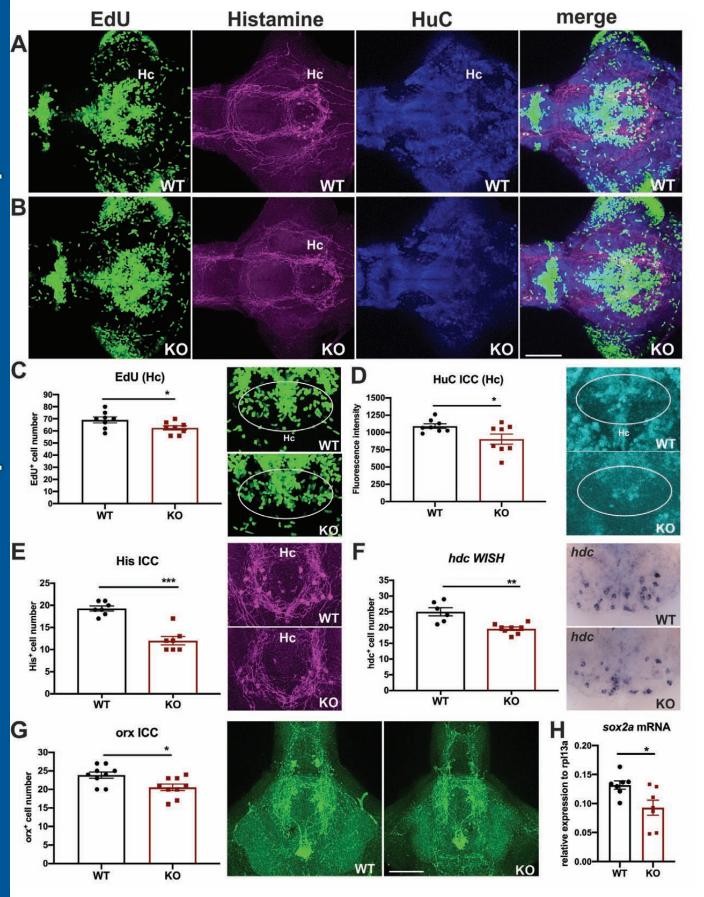




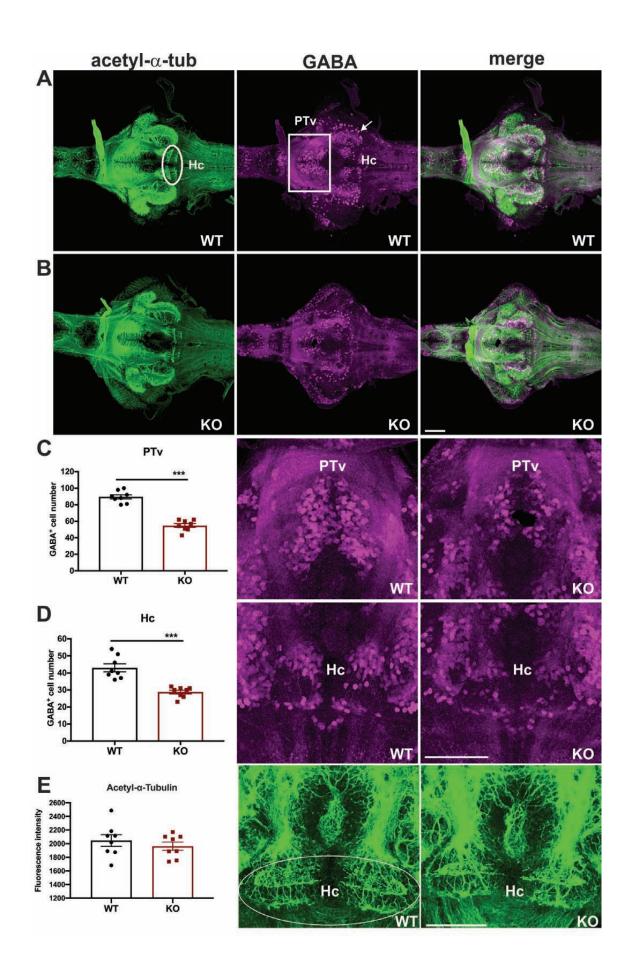




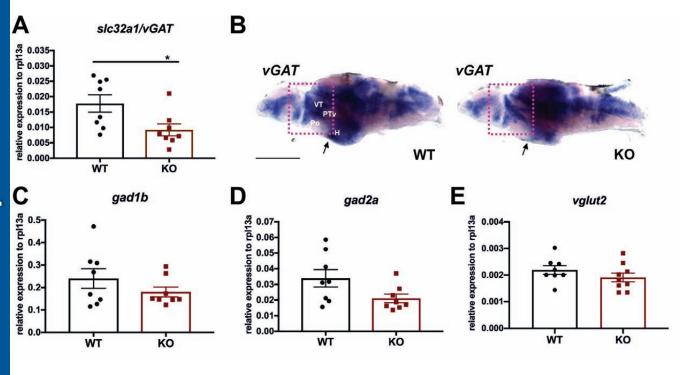




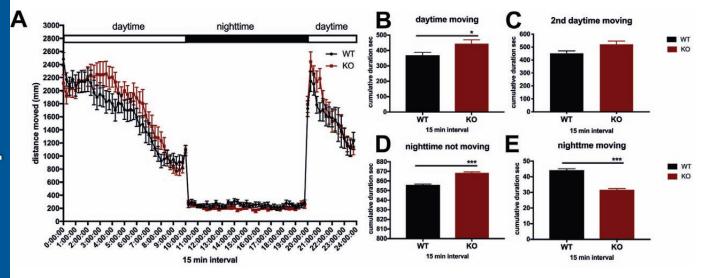




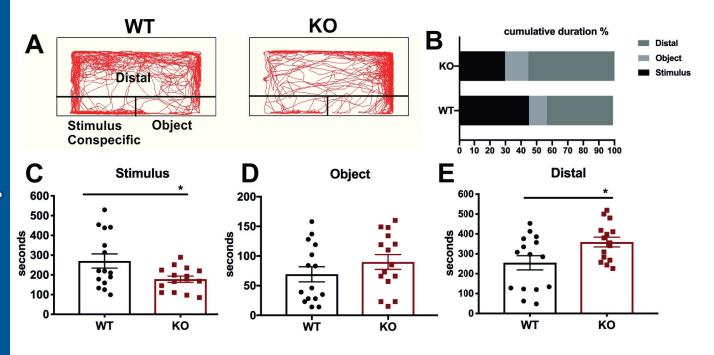




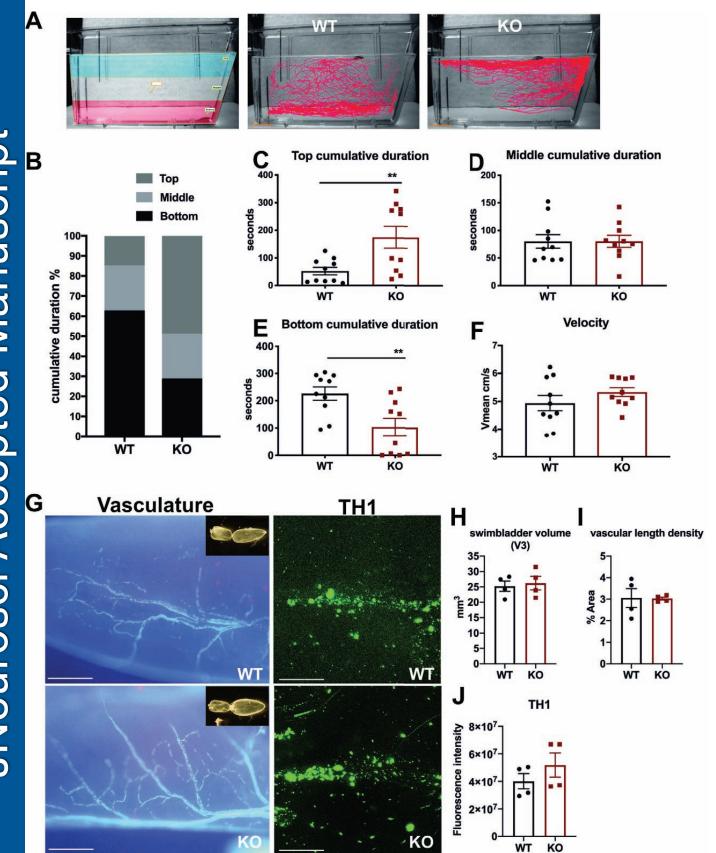












"<mark>`]</mark> Made Will Pdf Office

